

1 **Establishment of CRISPR/Cas9-based knock-in in a hemimetabolous insect: targeted gene**  
2 **tagging in the cricket *Gryllus bimaculatus***

3

4 Yuji Matsuoka<sup>1,3\*</sup>, Taro Nakamura<sup>2,4\*</sup>, Takahito Watanabe<sup>1,5</sup>, Austen A. Barnett<sup>2,6</sup>, Sumihare  
5 Noji<sup>7</sup>, Taro Mito<sup>1\*</sup>, Cassandra G. Extavour<sup>2,8\*</sup>

6

7 1. Department of Life Systems, Institute of Technology and Science, the University of  
8 Tokushima Graduate School, 201 Minami-Jyosanjima-cho, Tokushima City, 770-8506, Japan

9 2. Department of Organismic and Evolutionary Biology, 16 Divinity Avenue, Cambridge MA  
10 02138, USA

11 3. Department of Biological Sciences, National University of Singapore, 14 Science Drive 4  
12 117543, Singapore

13 4. Current address: National Institute for Basic Biology, Nishigonaka 38, Myodaiji, Okazaki 444-  
14 8585, Aichi, Japan

15 5. Bio-Innovation Research Center, Tokushima University, 2272-2 Ishii, Ishii-cho, Myozai-gun,  
16 Tokushima 779-3233, Japan

17 6. Current address: DeSales University, 2755 Station Avenue, Center Valley, PA 18034, USA

18 7. Tokushima University, 2-14 Shinkura-cho, Tokushima City, 770-8501, Japan

19 8. Department of Molecular and Cellular Biology, 16 Divinity Avenue, Cambridge MA 02138,  
20 USA

21

22 \* **Correspondence to:** Yuji Matsuoka [dbsyuji@nus.edu.sg](mailto:dbsyuji@nus.edu.sg)

23 Taro Nakamura [taro@nibb.ac.jp](mailto:taro@nibb.ac.jp)

24 Taro Mito [mito.taro@tokushima-u.ac.jp](mailto:mito.taro@tokushima-u.ac.jp)

25 Cassandra G. Extavour [extavour@oeb.harvard.edu](mailto:extavour@oeb.harvard.edu)

26

27 **Running Title:** CRISPR/Cas9 knock-ins in a cricket

28 **Abstract**

29 Studies of traditional model organisms like the fruit fly *Drosophila melanogaster* have contributed  
30 immensely to our understanding of the genetic basis of developmental processes. However, the  
31 generalizability of these findings cannot be confirmed without functional genetic analyses in  
32 additional organisms. Direct genome editing using targeted nucleases has the potential to transform  
33 hitherto poorly-understood organisms into viable laboratory organisms for functional genetic study.  
34 To this end, here we present a method to induce targeted genome knock-out and knock-in of desired  
35 sequences in an insect that serves as an informative contrast to *Drosophila*, the cricket *Gryllus*  
36 *bimaculatus*. The efficiency of germ line transmission of induced mutations is comparable to that  
37 reported for other well-studied laboratory organisms, and knock-ins targeting introns yields viable,  
38 fertile animals in which knock-in events are directly detectable by visualization of a fluorescent  
39 marker in the expression pattern of the targeted gene. Combined with the recently assembled and  
40 annotated genome of this cricket, this knock-in/knock-out method increases the viability of *G.*  
41 *bimaculatus* as a tractable system for functional genetics in a basally branching insect.

42

43 **Keywords:** CRISPR/Cas9, Orthoptera, genome editing, Hox genes, *Ultrabithorax*, *abdominal-A*

44

45

## 46 **Introduction**

47 In what is often called the “post-genomic era,” (Wainberg et al., 2021), massive advances  
48 in nucleic acid sequencing chemistry over the last two decades have given scientists access to  
49 greater volumes of gene sequence data than ever before (Kulski, 2016; Papageorgiou et al., 2018).  
50 However, this wealth of genomic information has highlighted two major gaps in our understanding  
51 of gene function and evolution. First, comparative genomic data and increased taxon sampling in  
52 functional genetic, developmental and cellular biology have revealed that the biology of many  
53 traditional laboratory model organisms is not representative of the broader clades to which they  
54 belong (Goldstein and King, 2016). Second, our ability to deduce accurately gene function from  
55 sequence data is limited to those genes that display high sequence and structural conservation  
56 (Ashburner et al., 2000; Consortium et al., 2020), and tools for manipulating gene function have  
57 been developed for only a small fraction of organisms (Russell et al., 2017). Addressing these  
58 problems calls for both increased taxon sampling and development of techniques to enable targeted  
59 alteration of gene function in understudied organisms. Here we address both of these issues by  
60 developing a method for targeted genome editing, including both knock-out and knock-in editing,  
61 in a basally branching insect model organism, the cricket *Gryllus bimaculatus*.

62 *G. bimaculatus* is an emerging model organism in a variety of fields of biology (Horch  
63 et al., 2017a; Kulkarni and Extavour, 2019). Ease of husbandry (Horch et al., 2017b), detailed  
64 developmental staging tables (Donoughe and Extavour, 2016), established gene expression  
65 analysis methods (Horch et al., 2017b), and an assembled and annotated genome (Ylla et al., 2021)  
66 make this cricket a highly amenable hemimetabolous laboratory model system (Kulkarni and  
67 Extavour, 2019). The developmental biology of *G. bimaculatus* has been of special interest, as in  
68 contrast to the ontogenetically derived model *Drosophila melanogaster*, many aspects of cricket  
69 embryogenesis are thought to resemble putative ancestral developmental modes of insects (Davis  
70 and Patel, 2002). For example, the function of several axial patterning genes has been analyzed  
71 and compared to that of their *D. melanogaster* homologues, revealing that the gene regulatory  
72 networks governing axial patterning have undergone considerable evolutionary change across  
73 insects (Matsuoka et al., 2015; Mito et al., 2007; Mito et al., 2008). *G. bimaculatus* is also used  
74 for the analysis of gene function in tissue regeneration (Bando et al., 2013; Mito et al., 2002;  
75 Nakamura et al., 2007), as this cricket can regenerate amputated organs, including legs and  
76 antennae, after several rounds of juvenile molts. In addition, *G. bimaculatus* is also used for the  
77 analysis of gene function and neuronal circuits in neuronal activity, including learning, memory

78 and circadian clocks (Hedwig and Sarmiento-Ponce, 2017; Matsumoto et al., 2018; Mizunami and  
79 Matsumoto, 2017; Tomiyama et al., 2020). Moreover, several species of cricket are being farmed  
80 as a new food source for humans because of their high protein and nutrient content (Huis et al.,  
81 2013).

82 Genome editing techniques using artificial nucleases were previously established in *G.*  
83 *bimaculatus* (Watanabe et al., 2012). However, construction of artificial nucleases is laborious.  
84 More recently, use of the clustered regulatory interspaced short palindromic repeat  
85 (CRISPR)/associated Cas9 nuclease (CRISPR/Cas9) has emerged and been verified as an efficient  
86 tool for genome editing in several arthropod species (Gilles et al., 2015; Gratz et al., 2013; Kistler  
87 et al., 2015; Li et al., 2015; Martin et al., 2016; Zhang et al., 2017). Here we briefly review this  
88 technique, investigate and demonstrate its utility for targeted genome modification in *G.*  
89 *bimaculatus*.

90 The CRISPR system is thought to have its ancestry in adaptable immune mechanisms  
91 used by many bacteria, which protect the genome from invasion by viruses (Amitai and Sorek,  
92 2016). The type II CRISPR system from *Streptococcus pyogenes* was adopted for sequence-  
93 specific introduction of double strand breaks in other organisms (Jinek et al., 2012). The  
94 CRISPR/Cas9 system is comprised of the Cas9 nuclease and a short guide RNA (sgRNA), which  
95 consists of a Cas9 interaction site and a target recognition site. By changing the sequence of the  
96 target recognition site, in principle any sequence in the genome can be targeted. However, in  
97 practice there are several constraints on experimental design in this system to optimize the function  
98 and specificity of sgRNAs. For example, a protospacer adjacent motif (PAM) located in the 3'  
99 downstream region of the target sequence is needed for interaction of sgRNA with Cas9 nuclease  
100 (Jinek et al., 2012). Recently, several additional factors that can impact the specificity and  
101 efficiency of sgRNA in several systems have been reported, including the number and positions of  
102 mismatches, and GC content (Hsu et al., 2013).

103 In the CRISPR/Cas9 system, sgRNAs recruit Cas9 nuclease to the target sequence, and  
104 Cas9 then introduces a double strand break (DSB) at the target sequence. The presence of DSBs  
105 triggers the activity of the cell's DNA repair machinery, non-homologous end joining (NHEJ), or  
106 homology directed repair (HDR). NHEJ is an error-prone machinery, such that insertions or  
107 deletions can be generated at the break point (Branzei and Foiani, 2008). By utilizing artificial  
108 nucleases to trigger NHEJ, we previously succeeded in generating mutant lines in *G. bimaculatus*  
109 (Watanabe et al., 2012). HDR, however, would be offer a more precise repair machinery, as the

110 break is repaired through use of a homologous template. By supplying a donor template containing  
111 sequence homologous to the target, in principle a desired donor sequence can be integrated into  
112 the genome through HDR. Such gene knock-ins, while highly desirable for detailed analysis of the  
113 function of genomic regions, are more difficult to achieve than gene knock-outs because of the  
114 low efficiency of HDR in eukaryotes (Hagmann et al., 1998), and although success with HDR has  
115 been reported in some insects including silk moth (Ma et al., 2014; Zhu et al., 2015), multiple  
116 mosquito species (Gantz et al., 2015; Hammond et al., 2016; Kistler et al., 2015; Purusothaman et  
117 al., 2021) and mosquito cell lines (Rozen-Gagnon et al., 2021) and the beetle *Tribolium castaneum*  
118 (Gilles et al., 2015), our attempts at HDR-based knock-in techniques have never succeeded in  
119 *Gryllus* (unpublished observations). Recently, an efficient gene knock-in method through NHEJ  
120 was developed in the zebrafish *Danio rerio* (Auer et al., 2014). In this method, both the genome  
121 and the donor vector are cleaved *in vivo*, then the terminal genomic and donor sequences are  
122 combined through NHEJ. The method is efficient and can integrate longer constructs into the  
123 genome than knock-ins achieved through HDR (Auer et al., 2014). Bosch and colleagues (Bosch  
124 et al., 2019) subsequently reported that this knock-in strategy also works in *D. melanogaster*.

125 Here, we present evidence that CRISPR/Cas9 system functions efficiently in *G.*  
126 *bimaculatus*, and that the efficiency of targeted gene disruption is much higher than that achieved  
127 using artificial nucleases. We demonstrate the utility of this technique for developmental biology  
128 by performing functional analysis of the *G. bimaculatus* orthologues of the Hox genes  
129 *Ultrabithorax* (*Gb-Ubx*) and *abdominal-A* (*Gb-abd-A*). Furthermore, using a donor vector  
130 containing an autonomous expression cassette, we demonstrate that gene knock-in by a homology-  
131 independent method works efficiently in *G. bimaculatus*. We show that this homology-independent  
132 gene knock-in method can be applied to identify mutant individuals simply by detecting marker  
133 gene expression. Efficient targeted genome editing, now including both knock-out and knock-in  
134 techniques, will pave the way for making this cricket a much more sophisticated model animal for  
135 functional genetic laboratory studies.

136

## 137 **Results**

138

### 139 *Targeted mutagenesis of the Gb-lac2 locus*

140 To determine whether the CRISPR/Cas9 system was functional in the cricket, we first tried to  
141 perform a targeted gene knock-out of the *laccase 2* (*Gb-lac2*) gene (Table 1), which regulates

142 tanning of the arthropod cuticle following molting (Arakane et al., 2005). We chose this gene  
143 because of its easily detectable loss of function phenotype, and because we had previously  
144 successfully generated stable mutant lines for this gene by using artificial nucleases (Watanabe et  
145 al., 2012). sgRNA target sites were first determined using the ZiFit online tool (Sander et al., 2010),  
146 and then we chose the target sequence from among these candidate sequences based on the number  
147 of mismatches relative to the other sequences on the genome (< 3 mismatches in the whole sgRNA  
148 sequence) and GC content ( $70 \pm 10\%$  for the whole sgRNA sequence). Based on these criteria,  
149 we designed sgRNAs against the fifth exon of *Gb-lac2*, which is close to the target regions of the  
150 previous artificial nuclease experiment (Fig. 1D; Table 2) (Watanabe et al., 2012).

151 We co-injected 0.5  $\mu\text{g}/\mu\text{l}$  sgRNA and 0.5  $\mu\text{g}/\mu\text{l}$  of Cas9 mRNA into 128 fertilized cricket  
152 eggs within 1-3 h after egg laying (AEL) (Table 3). Five days after injection, we evaluated the  
153 frequency of mutant alleles in individual eggs using the Surveyor<sup>TM</sup> nuclease assay (Qiu et al.,  
154 2004); see Materials and Methods for detailed mechanism and procedure). For sgRNA #1, we  
155 detected cleaved fragments of the expected sizes in all X examined eggs (Fig.1C), and for sgRNA  
156 #2, we detected these fragments in 13 out of 29 eggs examined (Table 3).

157 We observed mosaic pigmentation of the cuticle in 92% of G<sub>0</sub> hatchlings that emerged  
158 from the individual eggs injected with sgRNA#1, and in 44% of G<sub>0</sub> hatchlings that emerged from  
159 individuals injected with sgRNA #2, consistent with Cas9-mediated interruption of the *Gb-lac2*  
160 gene in some, but not all, somatic cells of the G<sub>0</sub> hatchlings raised these hatchlings to adulthood  
161 (Fig.1A). We crossed these G<sub>0</sub> adults with wild type crickets of the opposite sex, to determine the  
162 efficiency of germ line transmission of the Cas9-induced *Gb-lac2* mutations to the G<sub>1</sub> generation.  
163 We found that 77% of the mosaic G<sub>0</sub>s injected with sgRNA#1, and 20% of those injected with  
164 sgRNA#2, transmitted the mutation to their offspring (Fig.1B). To determine the nature of the *Gb-*  
165 *lac2* Cas9-induced alleles, we isolated genomic DNA from each line and analyzed the sequence of  
166 the *Gb-lac2* locus. We found that several different types of indel mutation were introduced at the  
167 target locus (Fig.1D). These results indicate that this CRISPR/Cas9-mediated genome editing  
168 system is functional in the cricket.

169  
170 *Targeted mutagenesis of the Gb-Ubx locus via knock-out*

171 To compare phenotypes obtained with targeted gene disruption to those obtained with the RNA  
172 interference (RNAi) method that has hitherto been the most common method of performing  
173 functional genetics in this cricket (Mito and Noji, 2008), we used the CRISPR/Cas9 system to

174 perform functional analyses of the *G. bimaculatus* ortholog of the Hox gene *Ultrabithorax* (*Gb-*  
175 *Ubx*) (Table 1). RNAi-induced phenotypes for *Gb-Ubx* have been previously examined in  
176 developing abdominal segments (Barnett et al., 2019; Matsuoka et al., 2015), providing a basis for  
177 comparison with CRISPR-induced mutants. We designed sgRNA for a sequence within an exon  
178 upstream of the homeodomain (Fig.2A), and co-injected 0.5 µg/µl of this sgRNA and 1 µg/µl Cas9  
179 mRNA into 167 fertilized cricket eggs within 1-3 h AEL. Seven days following injection, we  
180 extracted genomic DNA and performed the Surveyor™ assay to determine the efficiency of gene  
181 targeting. We found that *Gb-Ubx* mutations had been induced in all examined eggs (n=16) (Fig.2B).  
182 The remaining 151 injected G<sub>0</sub> embryos gave rise to ten adults, which we backcrossed to wild type  
183 adults of the opposite sex. We randomly chose approximately 30 G<sub>1</sub> eggs from each of the ten G<sub>0</sub>  
184 crosses, extracted genomic DNA from the pooled embryos, and performed the SURVEYOR  
185 Surveyor™ assay. We found that six out of ten G<sub>0</sub> crickets transmitted *Gb-Ubx* mutations to the  
186 next generation. We selected one of the G<sub>1</sub> *Gb-Ubx*<sup>CRISPR</sup> lines, which had a frame-shift mutation  
187 in the *Gb-Ubx* locus, for further phenotypic analysis. These *Gb-Ubx*<sup>CRISPR</sup> mutants displayed two  
188 different classes of phenotype: (1) *Contraction of the T3 leg*. Wild type *G. bimaculatus* adults have  
189 large, conspicuous T3 jumping legs. However, heterozygous mutants had smaller T3 legs than wild  
190 type (Fig.2C), and homozygous mutants obtained in the G<sub>2</sub> generation had T3 legs that were even  
191 smaller, almost the same size as T1/T2 legs (Fig.2C). These phenotypes were in good  
192 correspondence with those previously observed for *Ubx* RNAi in the cricket *Acheta domestica*  
193 (Mahfooz et al., 2007). (2) *Transformation of the A1 appendage*. Wild type *G. bimaculatus* germ  
194 band stage embryos possess two appendage-like organs on the A1 segment called the pleuropodia  
195 (Rathke, 1844; Wheeler, 1892). Instead of the pleuropodia present in wild type adults, the  
196 appendage outgrowths on the T1 segment of homozygous mutants were transformed towards leg-  
197 like structures (Fig.2D). This phenotype matches that previously observed in *Gb-Ubx* RNAi  
198 embryos (Barnett et al., 2019). In addition, in late embryos it was evident that an ectopic tergite  
199 was formed on the A1 segment of these mutants (Fig.2C). *Gb-Ubx*<sup>CRISPR</sup> heterozygous mutants are  
200 fertile but homozygous mutants were lethal. Therefore, to maintain this line, *Gb-Ubx*<sup>CRISPR</sup>  
201 heterozygous mutants were crossed to each other, and we performed the SURVEYOR Surveyor™  
202 assay to isolate heterozygous mutants.

203 To confirm whether the production of Gb-Ubx protein was indeed disrupted by these  
204 CRISPR-induced mutations, we performed immunostaining with the “UbdA” monoclonal  
205 antibody FP6.87 (Kelsh et al., 1994), which recognizes both Ubx and Abd-A proteins, and was

206 previously reported to cross-react in multiple *Gryllus* species including *G. bimaculatus* (Barnett et  
207 al., 2019; Mahfooz et al., 2004). In wild type embryos, the UbdA antibody revealed the expected  
208 combination of the Gb-Ubx and Gb-Abd-A expression patterns (Barnett et al., 2019; Mahfooz et  
209 al., 2004) (Fig.2D). In *Gb-Ubx<sup>CRISPR</sup>* embryos, however only the Gb-Abd-A expression domain  
210 was detected, while Gb-Ubx expression was clearly absent (Fig.2D), suggesting that the CRISPR-  
211 induced *Gb-Ubx* mutations interfered with Gb-Ubx protein production. To address the possibility  
212 of off-target CRISPR-mediated gene disruptions, we compared the abdominal appendage  
213 phenotypes of *Gb-Ubx<sup>CRISPR</sup>* embryos with those of *Gb-Ubx<sup>RNAi</sup>* embryos. Both types of embryos  
214 displayed similar phenotypes, namely moderate outgrowth of leg-like structures on the A1 segment,  
215 which normally generates pleuropodia rather than walking legs (Fig.2D). Taken together, these  
216 results suggest that the CRISPR/Cas9 system induced mutations specifically into the *Gb-Ubx* locus,  
217 which disrupted *Gb-Ubx* function.

218

219 *In-depth analysis of mutagenesis profile for the CRISPR/Cas9 system in G. bimaculatus*

220 To optimize the genome editing procedure, we wished to evaluate how the timing of injection  
221 affected NHEJ mutagenesis. For detailed assessment of this mutagenesis, we therefore performed  
222 in-depth analysis of the CRISPR mutants using next generation sequencing.

223 Our previous study had revealed early cellular dynamics during cricket embryogenesis  
224 (Nakamura et al., 2010), allowing us to assess whether specific mutagenesis events were correlated  
225 with cellular behaviors during early development. As in *D. melanogaster* (Foe and Alberts,  
226 1983) early mitotic divisions in *G. bimaculatus* embryos are syncytial, meaning that mitosis takes  
227 place without cytokinesis, resulting in multiple energids (nuclei surrounded by aqueous cytoplasm  
228 but lacking a unique lipid bilayer) within a single cell membrane (Donoughe and Extavour, 2016;  
229 Nakamura et al., 2010; Sarashina et al., 2003). To evaluate whether and how the timing of injection  
230 affected mutagenesis outcomes, we chose four early embryonic time points following the one-hour  
231 embryo collection period, as follows (Supplementary Fig.2A): (1) At the 1h injection time point,  
232 energids start to migrate from the center of the egg to the cortex. (2) At the 3h injection time point,  
233 energids continue to become distributed throughout the yolk, accompanied by mitotic cycles. (3)  
234 At the 5h injection time point, energids have become nearly uniformly distributed throughout the  
235 egg cortex and begin tangentially oriented nuclear division. (4) The 9h injection time point is one  
236 to eight hours before cellularization (Donoughe and Extavour, 2016). We co-injected 0.5  $\mu\text{g}/\mu\text{l}$  of  
237 the *Gb-Ubx* sgRNA, the Gb-lac2 sgRNA or an sgRNA targeting abdominal-A (*Gb-abd-A*); see



238 “*Knock-in of donor vector sequence at the Gb-abd-A locus*” below) described above, and 1 µg/µl  
239 of Cas9 mRNA into the eggs at each of these time point. At 5d AEL, genomic DNA was isolated  
240 from three individual embryos for each injection time point and used for amplicon sequencing. We  
241 examined the on-target site and the single highest predicted potential off-target site for each of the  
242 *Gb-Ubx* and *Gb-abd-A* genes. For each sample we performed amplicon sequencing with three  
243 replicates.

244 For *Gb-Ubx* on-target genome disruptions, we found that the rate of NHEJ-induced  
245 mutations decreased with the age of the embryo at injection (Supplementary Fig.2B). The same  
246 trend was also observed for *Gb-abd-A* on-target mutations (Supplementary Fig.2D; see section  
247 “*Targeted mutagenesis of the Gb-abd-A locus via knock-in*” below). This result is well correlated  
248 with the phenotypic severity observed in the G<sub>0</sub> hatchlings emerging from the *Gb-lac2*<sup>CRISPR</sup>  
249 embryos. *Gb-lac2*<sup>CRISPR</sup> embryos injected at the two earlier time points (1h and 3h) gave rise to  
250 hatchlings with broad mutated white patches of cuticle (Supplementary Fig.2H). In contrast, the  
251 embryos injected at 5h showed milder phenotypes (Supplementary Fig.2H) and the embryos  
252 injected at 9h showed only little detectable phenotype (Supplementary Fig.2H). For both *Gb-abd-*  
253 *A* and *Gb-Ubx* genes, the rate of NHEJ-induced mutations at the studied off-target site was less  
254 than 1.3% for all injection time points (Supplementary Fig.2C and 2E), suggesting that off-target  
255 effects may be minimal in this system.

256

#### 257 *Knock-in of donor vector sequence at the Gb-Ubx locus*

258 In addition to targeted sequence deletions, targeted sequence knock-in is a highly  
259 desirable technique that would expand our ability to understand the functions of genomic regions  
260 of interest. We had previously attempted to achieve targeted gene knock-ins through homology-  
261 dependent repair, but this method has not worked in *Gryllus* in our hands to date (data not shown).  
262 In a homology-independent knock-in method reported for *D. rerio* and *D. melanogaster* (Auer et  
263 al., 2014; Bosch et al., 2019), both genome and donor vector are cleaved *in vivo*, then the cut ends  
264 of genome and donor vector are combined through NHEJ. This method is more efficient than the  
265 homology-dependent method, potentially because NHEJ is highly active throughout the cell cycle  
266 in eukaryotes (Hagmann et al., 1998). However, due to the nature of NHEJ, the orientation of  
267 integration of the donor vector sequence cannot be controlled. In addition, indel mutations are  
268 generated at the junction point. To try to circumvent these issues, which might otherwise prevent  
269 functional knock-in, we generated a donor vector containing an autonomous expression cassette

270 comprising the *Gryllus actin* (*Gb-act*) promoter followed by the *eGFP* coding sequence  
271 (Nakamura et al., 2010). As a sgRNA recognition site, we included a partial *DsRed* gene sequence  
272 (Auer et al., 2014), which is native to the coral *Discosoma sp.* (Baird et al., 2000) and not present  
273 in the cricket genome. We predicted that successful knock-in of this donor sequence into the  
274 genome would result in GFP expression being driven by the *Gb-act* promoter regardless of the  
275 insert's orientation or any potential induced indel mutations. To try to further increase the utility  
276 of this tool to facilitate identification of targeted gene disruptions, we targeted knock-in of the  
277 donor sequence to an exon of the target gene, which we anticipated would result in disruption of  
278 target gene function. Our goal was to be able to identify such successfully knocked-in individuals  
279 by detectable GFP expression in the known expression domains of the target gene.

280 We targeted the *Gb-Ubx* locus for this targeted knock-in strategy and used the same  
281 sgRNA as that used for the knock-out experiment described above (see section “*Targeted*  
282 *mutagenesis of the Gb-Ubx locus via knock-out*”, Fig.2A; Fig.3A). We co-injected 50 ng/μl of  
283 sgRNA for *Ubx* locus, 50 ng/μl of sgRNA for donor vector, 100 ng/μl of Cas9 mRNA, and 100  
284 ng/μl of donor vector into fertile cricket eggs. By seven days after injection, four out of 85 injected  
285 embryos (4.7%) showed mosaic GFP expression in the T3 trunk and leg (Fig.3B). Of the 85  
286 injected embryos, 18 individuals (21.2%) grew to adulthood. We crossed them individually with  
287 wild type counterparts of the opposite sex and evaluated GFP expression in their offspring. One  
288 out of these 18 *G<sub>0</sub>* crickets (5.6%) produced embryos with GFP expression in a pattern identical to  
289 that of *Gb-Ubx* (Barnett et al., 2019; Matsuoka et al., 2015; Zhang et al., 2005) (Fig.3B). The GFP  
290 expression was detectable through the eggshell even at late embryonic stages. At adult stages,  
291 knock-in crickets showed detectable GFP expression in the hind wing and T3 legs (Supplementary  
292 Fig.3A).

293 To confirm the integration of donor sequence into the genome, we performed PCR and  
294 sequence analysis. We designed specific primers for each 5' and 3' junction point (Fig.3A). All XX  
295 examined embryos showed the expected amplicon size for both junctions (Fig.3D), suggesting that  
296 at least two copies of the donor vector fragment were integrated into the genome. Sequence  
297 analysis further confirmed the integration of the donor plasmid into the genome, and that indel  
298 mutations were generated at each junction (Fig.3E). We also performed copy number estimation  
299 by real-time quantitative PCR. The expression level of GFP was normalized to the expression level  
300 of the endogenous *orthodenticle* gene, which is known to have only one copy in the genome  
301 (Nakamura et al., 2010; Ylla et al., 2021). The results of this analysis indicated that four copies of

302 the donor plasmid were integrated into the genome (Supplementary Fig.4A).

303 To determine whether the function of the target gene was indeed disrupted by this  
304 Knock-in/Knock-out strategy, we examined GFP expression and morphology in G<sub>1</sub> *Gb-Ubx*<sup>CRISPR-</sup>  
305 <sup>KI</sup>embryos. Among the G<sub>1</sub> *Gb-Ubx*<sup>CRISPR-KI</sup>embryos, we found they displayed one of two different  
306 intensities of GFP expression (Fig.3C). Some crickets showed weak GFP expression and displayed  
307 no detectable morphological abnormalities (Fig). The crickets with strong GFP expression,  
308 however, had smaller T3 legs and formed leg-like structures rather than pleuropodia on the A1  
309 segment (Fig). These phenotypes, which were the same as those observed in the *Gb-Ubx*  
310 homozygous mutant (Fig.2C), suggested that the weak GFP expression crickets may be  
311 heterozygous mutants, and the strong GFP expression crickets may be homozygous mutants.

312

313 *Knock-in of donor vector sequence at the Gb-abd-A locus*

314 To confirm the efficiency and utility of this method, we next chose the Hox gene *Gb-*  
315 *abdominal-A* (*abd-A*) as a target (Table 1). We designed sgRNAs for the sequence within the exon  
316 just upstream of the homeodomain (Fig.4A). We co-injected 50 ng/μl of sgRNA for the *Gb-abd-A*  
317 locus, 50 ng/μl of sgRNA for the donor vector, 100 ng/μl of Cas9 mRNA, and 100 ng/μl of donor  
318 vector into fertilized cricket eggs.

319 Of 38 injected G<sub>0</sub> embryos, five showed mosaic GFP expression in the abdomen (Fig.4B).  
320 Four G<sub>0</sub> adults were individually backcrossed with wild type counterparts of the opposite sex to  
321 obtain multiple G<sub>1</sub> crickets. We obtained one stable transgenic line, in which GFP expression in  
322 G<sub>2</sub> embryos was similar to the previously documented expression pattern of *Gb-abd-A* transcript  
323 (Barnett et al., 2019; Matsuoka et al., 2015; Zhang et al., 2005) (compare Fig.4B with  
324 Supplementary Fig.1C). In a replicate injection experiment, we obtained a second such transgenic  
325 line (Table 3). PCR and sequence analysis confirmed that one of the two lines contained the  
326 plasmid fragment in the sense orientation, and the second line contained the plasmid fragment in  
327 the antisense orientation (Fig.4C). Copy number estimation analysis results suggested that a single  
328 plasmid fragment was integrated into the genome in each line (Supplementary Fig.4).

329 In the *Gb-abd-A*<sup>KI-exon</sup> lines, GFP expression was detectable in nymphs even through the  
330 cuticle FIG. We further detected GFP expression in adult male and female internal organs. In wild  
331 type females, a pair of ovaries, each comprising hundreds of ovarioles, is located in the anterior  
332 abdomen (Nandchahal, 1972). Mature eggs are stored in an egg chamber at the posterior of each  
333 ovariole, and eggs are subsequently moved posteriorly through the oviduct. The posterior end of

334 the oviduct is connected to the uterus, where fertilization takes place, located at the base of the  
335 ovipositor (Supplementary Fig.5C”). In *Gb-abd-A*<sup>KI-exon</sup> mutant females, GFP expression was  
336 detected in the posterior portion of the oviduct (compare Supplementary Fig.5B’ and B” to  
337 Supplementary Fig.5A’). In *Gb-abd-A*<sup>KI-exon</sup> males, ubiquitous GFP expression was detected  
338 throughout the testis (compare Supplementary Fig.5E’ and E” to Supplementary Fig.5D’). The  
339 observed GFP expression in females is reminiscent of the expression pattern of *D. melanogaster*  
340 *abd-A* in the developing female genital disc (which gives rise to the somatic reproductive structures  
341 including the oviduct in this fruit fly (Epper, 1983; Sánchez and Guerrero, 2001), and in the adult  
342 oviducts (Foronda et al., 2006). *abd-A* expression has not, to our knowledge, been detected in the  
343 *D. melanogaster* male genital disc (Freeland and Kuhn, 1996), which gives rise to male somatic  
344 reproductive structures. However, high-throughput sequencing data from the modENCODE  
345 project do report *abd-A* expression in the adult *D. melanogaster* testis (Brown et al., 2014).

346

#### 347 *Targeted insertion of an expression cassette into an intron of the Gb-abd-A locus*

348 Kimura and colleagues (Kimura et al., 2014) demonstrated that in *D. rerio* the homology  
349 independent method could be applied for trapping endogenous enhancer activity by inserting a  
350 donor sequence containing an expression cassette into the 5’UTR of genes of interest. We aimed  
351 to apply this technique to *G. bimaculatus* by attempting to knock-in a donor vector into the intronic  
352 region of *Gb-abd-A* (Fig.5A).

353 We co-injected an sgRNA against an intron of *Gb-abd-A*, together with all other relevant  
354 reagents as described above (sgRNA against the donor vector, donor vector, and Cas9 mRNA). Of  
355 100 injected eggs, two eggs showed mosaic expression of GFP in the abdomen (Fig.5B). When  
356 the donor sequence was inserted into an exon in the previous experiment (see “*Knock-in of donor*  
357 *vector sequence at the Gb-abd-A locus*” above), GFP expression was accompanied by a phenotype  
358 of ectopic leg-like structure development on abdominal segments (Fig.5B, B’, B”), as previously  
359 observed in *Gb-abd-A* RNAi experiments (Barnett et al., 2019). However, when the plasmid  
360 fragment was inserted into an intron, the region expressing GFP did not generate ectopic leg-like  
361 structures (Fig.5C, C’, C”). This apparent absent or minimal loss of function phenotype in the  
362 intron knock-in embryos might explain the relatively high survival rate of the intron-targeted G<sub>0</sub>  
363 embryos (28% of injected G<sub>0</sub> embryos survived to adulthood) compared to that of the exon-targeted  
364 G<sub>0</sub> embryos (4.9% to 8.5% of XX injected embryos survived to adulthood; Table 3).

365 We obtained one *Gb-abd-A*<sup>KI-intron</sup> line, in which we confirmed that one donor vector  
366 sequence was integrated into the target region in a forward orientation (Fig). We carefully  
367 inspected the morphology of the *Gb-abd-A*<sup>KI-intron</sup> adult crickets to assess whether potential post-  
368 embryonic functions of the target gene were affected by insertion of the donor sequence into an  
369 intron. G<sub>1</sub> heterozygous *Gb-abd-A*<sup>KI-intron</sup> females did not show the supernumerary ovipositors  
370 observed in XX adults FIG, and they laid eggs normally (data not shown). For further confirmation,  
371 we examined the morphology of G<sub>2</sub> homozygous *Gb-abd-A*<sup>KI-intron</sup> mutants. Approximately 25%  
372 of examined G<sub>2</sub> eggs showed strong GFP expression, which we interpret is likely indicative of a  
373 homozygous mutant. All of these strong-GFP G<sub>2</sub> embryos generated leg-like structures on the  
374 abdomen (Fig.5E, E', E''), suggesting that the function of the target gene was somewhat affected  
375 in the homozygous condition, unlike in the mosaic condition exhibited by G<sub>0</sub> embryos FIG.

376

## 377 Discussion

378 In the present study, we demonstrated that targeted knockout and knock-in by using CRISPR/Cas9  
379 system works efficiently in the cricket *G. bimaculatus*. We performed functional analysis of  
380 CRISPR/Cas9-induced mutations in the Hox genes *Gb-Ubx* and *Gb-abd-A* during embryogenesis  
381 and at post-embryonic stages. We found that the cleavage efficiency of the CRISPR/Cas9 system  
382 was much higher than that previously reported for artificial nucleases in this cricket ((Watanabe et  
383 al., 2012; Watanabe et al., 2014)). We demonstrated that gene knock-in via a homology-  
384 independent method is effective in this cricket, and successfully applied it to functional analysis  
385 of Hox genes by knocking a donor sequence into an exon of the target gene to disrupt the function  
386 of the target gene (knock-in/knock-out). In addition, we succeeded in trapping endogenous gene  
387 activity using this method and revealed a number of new expression domains that had not been  
388 previously observed with traditional methods (Barnett et al., 2019; Matsuoka et al., 2015; Zhang  
389 et al., 2005)(Barnett et al., 2019; Matsuoka et al., 2015; Zhang et al., 2005). This homology-  
390 independent method is technically simpler than the homology-dependent methods, as the donor  
391 plasmid does not need to be newly made for each target region.

392

## 393 CRISPR/Cas9 system vs RNA interference

394 Delivering the proper amount of genome editing constructs at the proper time is important for  
395 efficient outcomes. For example, the embryos injected around 3h AEL, at which energids are  
396 distributing, were highly efficiently affected, but both detectable mosaic phenotypes (of *Gb-lac2*

397 crispants) and the rate of NHEJ decreased with later injections at blastoderm stages  
398 (Supplementary Fig.2H). Furthermore, the efficiency of knock-in was much lower than that of  
399 knockout FIG. Thus, we suggest that further optimization of delivery conditions can be achieved  
400 by using pigmentation genes as an index.

401 In our study, reproducibility and severity of phenotypes generated with the  
402 CRISPR/Cas9 were greater than those obtained with RNAi FIG. We speculate that the efficiency  
403 of RNAi-mediated knockdown may be influenced by when and at what levels the target gene is  
404 expressed. In the case of *Gb-abdA* and *Gb-Ubx*, these genes are expressed much later in  
405 development (stage) than the stage at which we perform injections (stage). Correspondingly, much  
406 higher concentrations of dsRNA have proven necessary to produce even mild phenotypes (5-6  
407  $\mu\text{g}/\mu\text{l}$ ; Fig.2D), than those typically used for RNAi against most genes in this cricket (1-2  $\mu\text{g}/\mu\text{l}$ ;  
408 e.g. Donoughe et al., 2014). In contrast, early indel mutations generated by genome editing  
409 techniques resulted in clearly detectable, severe phenotypes FIG. Several studies have  
410 demonstrated that genome editing techniques can sometimes be adequate for functional analysis  
411 of target genes in mosaic  $G_0$  individuals (e.g. Daimon et al., 2015; Martin et al., 2016; Matsuoka  
412 and Monteiro, 2018). However, it is often difficult or impossible to unambiguously identify mutant  
413 cells in such mosaics. In this regard, establishment and maintenance of stable mutant lines as  
414 performed herein, allows for less ambiguous phenotypic analysis in this cricket.

415 Although the CRISPR/Cas9 system is efficient, it offers little to no conditionality, which  
416 can complicate study of the many genes that act pleiotropically during development (Minelli,  
417 2016). For example, in the case of *Gb-abd-A*, the gene acts to repress leg formation in the abdomen  
418 at embryonic stages (Supplementary Fig.6), while at adult stages, it regulates proper development  
419 of female genitalia (Supplementary Fig.5). Likely because of this latter phenotype, we were unable  
420 to obtain homozygous *Gb-abdA*<sup>CRISPR</sup> animals. To overcome this problem, sophisticated genetic  
421 methods, like balancer chromosomes (Miller et al., 2019), will need to be developed in the future.  
422 In this regard, RNAi offers more options for conditional control of gene function. By controlling  
423 the timing of injection of dsRNA, target gene activity can be knocked down at any desired  
424 developmental stage in *G. bimaculatus* (Dabour et al., 2011; Nakamura et al., 2008; Takahashi et  
425 al., 2009). Thus, while the CRISPR/Cas9 system is a powerful new tool for gene function analyses,  
426 RNAi remains a useful technique for this system.

427

428 *Application of homology independent knock-in method for functional analysis of endogenous*  
429 *genes*

430 Homology-independent knock-in methods will expand our ability to analyze the  
431 function of target genes in this hemimetabolous insect model. Here, we demonstrated one such  
432 application, the KI/KO method, which allows for isolation of mutants without PCR-based  
433 genotyping. When analyzing mutant phenotypes, affected individuals must typically be  
434 distinguished either by their morphology or by molecular methods to detect changes in target gene  
435 product levels or functions. In the case of the *Gb-Ubx* mutant, we would have needed to distinguish  
436 subtle differences in the T3 and A1 embryonic segments (Fig.2C), requiring destructive sampling.  
437 Moreover, antibodies against target genes may not be routinely available in many cases. The  
438 KI/KO method allows us to distinguish mutant individuals based on marker gene expression. Even  
439 heterozygous and homozygous mutants can sometimes be distinguished based on the intensity of  
440 marker gene expression. A similar strategy was employed in mosquitos via HDR (McMeniman et  
441 al., 2014). In the present study, we could easily identify the GFP expression resulting from the  
442 KI/KO event because it matched the previously characterized expression pattern for *Gb-Ubx*  
443 (Barnett et al., 2019; Matsuoka et al., 2015; Zhang et al., 2005). However, for target genes with  
444 previously uncharacterized expression domains, analysis may be more complex.

445 The promoter used in all expression cassettes herein is the same one used in a previous  
446 study to drive ubiquitous constitutive expression (Nakamura et al., 2010). Nevertheless, all  
447 knocked-in lines showed a spatially and temporally restricted GFP expression pattern like that of  
448 the target gene. We speculate that the promoter in the expression cassette acts as a minimal  
449 promoter, and that the observed GFP expression resulted from trapping endogenous enhancer  
450 activity. The GFP expression was not caused by the fusion to the endogenous gene product, since  
451 both the line containing an inverted orientation of the donor sequence, and the knock-in line  
452 targeting an intronic region, showed similar GFP expression patterns. To enhance the usefulness  
453 of this method, identification and use of a ubiquitous and strong promoter could in principle drive  
454 exogenous marker gene expression in the whole embryo without being subject to positional effects.

455 A remarkable feature of the homology-independent knock-in method is the length of  
456 sequence that can be integrated. In case of KI through HDR, a few kb of sequence can be integrated  
457 into the genome in arthropods (Gilles et al., 2015; McMeniman et al., 2014). In this study, through  
458 NHEJ, at least six kb of plasmid sequence was integrated into the genome. Furthermore, in some  
459 cases, four copies of plasmid sequence were integrated in tandem into the genome. In this case,

460 we speculate that first the donor plasmids were digested and combined via NHEJ, and then the  
461 combined fragment was knocked in into the genome via NHEJ, suggesting that homology-  
462 independent knock-in might be able to integrate several tens of kb of sequence into the genome. A  
463 recent study showed that a 200 kb BAC vector could be integrated into a rodent genome through  
464 a similar strategy (Yoshimi et al., 2016). This method might therefore be used for direct functional  
465 comparison of genomic regions by exchanging homologous regions between related species of  
466 interest.

467         The efficiency of knock-in through NHEJ is high, but to make improve its feasibility as  
468 a technique for functional genetic analysis in this cricket, future studies may be able to further  
469 enhance efficiency by optimizing at least one of three parameters, as follows: (1) *Enhance*  
470 *expression cassette copy number*. Empirically, G<sub>0</sub> crickets showing mosaic expression tend to  
471 transmit their knocked-in transgene to their offspring. To increase the efficiency of obtaining  
472 knock-in lines, future efforts should therefore focus on increasing the number of mosaic marker  
473 gene expression cassettes in G<sub>0</sub> embryos. Based on the results of our copy number estimation,  
474 there was variation in the number of vectors integrated into the genome, and the GFP expression  
475 level appeared correlated with the number of inserts. We also observed that some expression  
476 cassettes seemed to show higher expression levels than others and were therefore easier to detect  
477 in mosaic G<sub>0</sub>s. For example, the transgenic line containing one copy of the donor sequence within  
478 a *Gb-Ubx* intron had weaker GFP expression than the *Gb-abd-A* intronic knock-in line that also  
479 possessed one copy of the donor sequence FIG. We speculate that the *Gb-abd-A* locus might be  
480 able to drive higher gene expression than the *Gb-Ubx* locus. Inclusion of inducible expression  
481 elements such as a heat shock promoter or a modified Gal4/UAS system might help to enhance  
482 the activity of the expression cassette. (2) *Supply sgRNA and/or Cas9 nuclease via plasmid*.  
483 Recently, homology-dependent gene knock-in in the beetle *Tribolium T. castaneum* was reported  
484 (Gilles et al., 2015). In this protocol, both sgRNA and Cas9 nuclease were supplied from a donor  
485 plasmid. We speculate that consecutive production of Cas9 and sgRNA might contribute to the  
486 high efficiency of knock-ins reported in that study (Gilles et al., 2015) . In human cultured cells,  
487 the half-life of sgRNA drops to near-background levels by 4h after nucleofection, and earlier  
488 introduction of Cas9 mRNA attenuates sgRNA degradation because Cas9 protein functions to  
489 protect sgRNAs from degradation (Hendel et al., 2015). Alternatively, using Cas9 protein instead  
490 of mRNA might also improve efficiency in *G. bimaculatus*. (3) *Introduce insulator sequences into*  
491 *the donor cassette*. Positional effects might also in principle prevent the full potential activity of



492 the expression cassette. In this study, our vector plasmid contained insulators of the sea urchin  
493 *Hemicentrotus pulcherrimus* arylsulfatase gene (Takagi et al., 2011) on either side of the  
494 expression cassette (see Materials and Methods), but we nonetheless detected while GFP  
495 expression in a pattern matching that of the target gene. To achieve effective insulation, future  
496 studies might evaluate several different combinations of insulator orientations, which can affect  
497 insulator activity (Tchurikov et al., 2009). Alternatively, other insulators such as that of the *gypsy*  
498 retrotransposon (Modolell et al., 1983), might be additional options for future optimization  
499 (Carballar-Lejarazú et al., 2013).

500 In conclusion, we provide evidence that the CRISPR-Cas9 system works well in the  
501 cricket *G. bimaculatus*. In depth analysis of CRISPR-Cas9-induced mutations revealed optimized  
502 injection timing. In addition, we succeeded in the targeted functional knock-in of exogenous  
503 sequences into the genome through NHEJ.

504

## 505 **Materials and Methods**

506

### 507 *Cricket husbandry*

508 All adult and juvenile *Gryllus bimaculatus* were reared in plastic cages at 26–30 °C and 50%  
509 humidity under a 10-h light, 14-h dark photoperiod. They were fed on artificial fish food (Tetra)  
510 or Purina cat food (item #178046). For microinjections, fertilized eggs were collected on a wet  
511 kitchen towel in a plastic dish and incubated at 28 °C as previously described (Barry et al., 2019;  
512 Watanabe et al., 2017).

513

### 514 *Construction of sgRNA vectors*

515 For designing sgRNA, target sequences were designed with the ZiFit online tool (Sander et al.,  
516 2007; Sander et al., 2010). From the suggested candidates, we selected target sequences based on  
517 the number of mismatches (> 3 mismatches) and GC content (around 70%), as per Ren and  
518 colleagues (Ren et al., 2014). Off-target sites were designed using CasOT (Xiao et al., 2014). We  
519 modified the pDR274 vector (Addgene plasmid #42250) to expand its utility (the GGN<sub>18</sub>NGG  
520 sequence was present in the original pDR274, while in the modified vector, a GN<sub>19</sub>NGG sequence  
521 was used). Two synthetic oligonucleotides (5'-ATAG-N<sub>19</sub>-3' and 5'-AAA-N<sub>20</sub>) were annealed and  
522 inserted into the Bsa I site of the modified pDR274 vector. We confirmed insertion by Sanger  
523 sequence analysis.

524

### 525 *Synthesis of sgRNA and mRNA*

526 For sgRNA synthesis, the template for *in vitro* transcription was digested from the vectors  
527 generated as described above with DraI. For Cas9 mRNA synthesis, the template for *in vitro*  
528 transcription was digested from pMLM3613 (Addgene catalogue #42251) with PmeI. Both sgRNA  
529 and Cas9 mRNA were *in vitro* transcribed using mMESSAGE mMACHINE T7 Kit (Life  
530 Technologies catalogue #AM1344), and) and purified by ethanol precipitation. For the Cas9  
531 mRNA, we attached a poly-A tail by using a poly-A tailing Kit (Life Technologies catalogue  
532 #AM1350). The concentration of synthesized RNAs was estimated by NanoDrop and gel  
533 electrophoresis.

534

### 535 *Construction of donor plasmids*

536 The *eGFPbait-2A-RFP* donor plasmid was generated in a pUC57 vector by commercial artificial  
537 composition (GeneScript). The *DsRedbait-G'act-eGFP* donor plasmid was generated based on the  
538 *eGFPbait-2A-RFP* donor plasmid. First, 2A-RFP was digested using BglII and NotI. *Gb-act-eGFP*  
539 was also digested from a pXL-BacII- G'act-*eGFP* vector and ligated to generate the *eGFPbait-*  
540 *G'act-eGFP* vector. Then, we digested this *eGFPbait* vector using BglII and SacI. We amplified  
541 *DsRedbait* with primers (5' to 3') DsRed\_fwd: GCTCAGATCTCTTGGAGCCGTACTGGAAC,  
542 and DsRed-rev: GTACGAGCTCCATCACCGAGTTCATGCG. The amplicon was ligated to  
543 generate the *DsRedbait-G'act-eGFP* donor plasmid. The *DsRedbait-2×Ars\_rev-G'act-eGFP-*  
544 *2×Ars\_fwd* donor plasmid was generated based on the *DsRedbait-G'act-eGFP* donor plasmid. The  
545 Ars insulator sequence ArsInsC from *H. pulcherrimus* (Takagi et al., 2011) was amplified from an  
546 ArsInsC-containing plasmid (kind gift of Naoaki Sakamoto, Hiroshima University, Japan) and  
547 integrated on either side of the expression cassette in the donor plasmid.

548

### 549 *Microinjection*

550 Cas9 mRNA, sgRNA, and donor vectors were injected into 2-5h AEL cricket eggs. Cricket eggs  
551 were aligned in a groove 0.7 mm deep and 0.7 mm wide, made with 2% agarose in 1x phosphate-  
552 buffered saline (PBS) using a custom mold as previously described (Barry et al., 2019; Watanabe  
553 et al., 2017) and filled with 1xPBS. Needles for injection were made by pulling glass capillaries  
554 with filament (Narishige catalogue # GD-1) with a pipette puller (Sutter Instrument catalogue # P-  
555 1000IVF), using the following pulling program: (1) x3 Heat; 858, Pull; 0, Velocity; 15, Time; 250,

556 Pressure; 500, and (2) x1 Heat; 858, Pull; 80, Velocity; 15, Time; 200. To minimize the  
557 invasiveness of the injection, the tips of the pulled needles were sharpened and ground to a 20°  
558 angle by using a Micro Grinder (Narishige catalogue # EG-400). Approximately 5 nl of solution  
559 was injected into eggs with a Micro Injector (Narishige catalog # IM300). After injection, eggs  
560 were moved to a fresh Petri dish and submerged in fresh 1xPBS containing 50 U/ml penicillin and  
561 50 µg/ml streptomycin (15070-063, Thermo Fisher), and incubated at 28°C. During the incubation  
562 period, the 1xPBS with penicillin and streptomycin was replaced every day. We observed  
563 fluorescent protein expression at the stages when the target gene was known to be expressed.  
564 Genomic DNA was extracted from 7 d AEL eggs and adult T3 legs and used for insertion mapping  
565 and sequence analyses. After 2 days of incubation, injected cricket eggs were moved to wet filter  
566 paper in a fresh Petri dish for hatching.

567

#### 568 *Detection of indel mutations*

569 After Cas9 nuclease digests a target sequence, the disrupted sequence is repaired by either the  
570 NHEJ or the HDR cell machinery. To confirm a KO mutation, we searched for errors repaired by  
571 the NHEJ pathway, which sometimes induces or deletes nucleotides at the digested site during the  
572 repair process. Since disruption or repair are unlikely to take place identically in all cells of an  
573 injected G<sub>0</sub> embryo, G<sub>0</sub> animals are expected to contain heterogeneous sequences at the CRISPR  
574 targeted site, and thus to be heterozygous for a putative Cas9-induced indel. To confirm the activity  
575 of the sgRNAs, the SURVEYOR Surveyor™ Mutation Detection Kit (Transgenomic,) was used.  
576 This assay relies on a “surveyor” nuclease that can recognize and digest a heteroduplex DNA  
577 structure. First, genomic DNA was extracted from whole eggs or part of the T3 leg by a phenol  
578 chloroform method as previously described (Barry et al., 2019; Watanabe et al., 2017).  
579 Subsequently, approximately 200 bp of the targeted region was amplified by PCR from genomic  
580 DNA (Table 4). PCR conditions were optimized to reduce non-specific amplification or smearing.  
581 To create the putative heterogeneous DNA structure for the nuclease assay, the PCR product was  
582 heated to 98°C for five minutes, and then re-annealed by gradually cooling down to 30°C. Half of  
583 the PCR product was digested with the SURVEYOR Surveyor™ nuclease, and the other half was  
584 used as a negative control and incubated without the nuclease. Digestion was confirmed by agarose  
585 gel electrophoresis. For sgRNAs that yielded indels in the target sequence, digest of the PCR  
586 product by the Surveyor™ nuclease is expected to produce split fragments around the CRISPR  
587 targeted site relative to the negative control; the latter should not be digested by the nuclease and

588 thus should remain intact and run at the same size as the original amplicon. Positive PCR products  
589 were extracted from the gel, purified with the QIAquick Gel Extraction Kit (Qiagen catalogue  
590 #28506), and sub-cloned into the pGEM-Teasy vector (Promega catalogue #A1360) using TA-  
591 cloning. The vectors were used for Sanger sequence analysis.

592

#### 593 *Amplicon sequence analysis*

594 After a 1h egg collection, eggs were incubated for the desired length of time at 28°C. We co-  
595 injected 0.5 µg/µl sgRNA and 1 µg/µl Cas9 mRNA into fertilized cricket eggs after each of these  
596 incubation periods. Five days after injection, genomic DNA was extracted individually from three  
597 individual eggs from each of the four tested injection times; the latter analysis was performed in  
598 biological triplicate. Amplicon sequence analysis was performed by using MiSeq (Illumina), and  
599 the preparation of DNA libraries and sequencing reactions were performed according to the  
600 manufacturer's instructions. We read ~10,000 reads for on-target regions and ~50,000 reads for  
601 off-target regions. The assembly of output paired end reads was performed by using CLC Genomic  
602 Workbench (CLC Bio, QIAGEN Digital Insights). The relative proportions of reads containing  
603 indels and substitutions in the individual eggs were calculated with the online-tool CRISPResso  
604 (Pinello et al., 2016). We used the Integrative Genomic Viewer (Broad Institute) for investigation  
605 of the distribution of indels and substitutions (Thorvaldsdóttir et al., 2013).

606

#### 607 *Insertion mapping*

608 Genomic DNA was extracted from GFP-positive eggs of each line. Due to the specifics of this  
609 knock-in method, two types of insertion of vector fragment (sense and antisense orientations)  
610 would be expected to occur; we therefore performed PCR using primers designed against either  
611 side of the putative junction. PCR was performed using target region-specific (upstream or  
612 downstream of sgRNA recognition site) and donor vector-specific primers (sequence within *eGFP*  
613 for forward integration and M13Fw for reverse integration). Primer sequences are listed in Table  
614 4. Positive PCR products were extracted from the gel, purified by using the QIAquick Gel  
615 Extraction Kit (Qiagen catalogue #28506), and sub-cloned into the pGEM-Teasy vector (Promega  
616 catalogue #A1360) using TA-cloning. The vectors were used for Sanger sequence analysis.

617

#### 618 *Embryo fixation, whole mount in situ hybridization, and immunohistochemistry*

619 Embryos were dissected in 1xPBS and fixed with 4% paraformaldehyde PFA in 1xPBS + 0.1%  
620 Tween (PBT) for 1h at 4°C. The fixed embryos were dehydrated stepwise in 25%, 50%, 75%, and  
621 100% methanol in 1xPBT with five minutes per wash. The dehydrated embryos were stored in  
622 100% methanol at -30°C. Whole-mount *in situ* hybridization with digoxigenin (DIG)-labeled  
623 antisense RNA probes was performed as previously described (Niwa et al., 2000; Zhang et al.,  
624 2005). Immunohistochemistry was performed as follows: Fixed embryos were rehydrated stepwise  
625 in 75%, 50%, and 25% solutions of methanol/ PBT and finally in 100% PBT for five minutes in  
626 each solution. After blocking with 1% bovine serum albumin (BSA) (Thermo Fisher) in PBT for  
627 one hour at room temperature, embryos were incubated with an anti-UbdA antibody FP6.87 (Kelsh  
628 et al., 1994) (Developmental Studies Hybridoma Bank) diluted 1:200 in 1% BSA/PBT overnight  
629 at 4°C. After washing with PBT three times, embryos were incubated in 1% BSA/PBT for one  
630 hour at room temperature, and then incubated with Alexa Fluor 488-conjugated Goat Anti-mouse  
631 IgG(H+L) (Invitrogen catalogue #A32723) diluted 1:400 in 1% BSA/PBT for one hour at 4°C.  
632 After washing the embryos with PBT once for 10-60 minutes, embryos were counter-stained with  
633 DAPI (Sigma catalogue #10236276001) stock solution 1mg/mL diluted 1:1000 in PBT for ten  
634 minutes, and then washed with PBT two times for 10-60 minutes per wash. PBT was then  
635 substituted with 25% and 50% glycerol/PBT to clear embryos for microscopy.

636

### 637 *Copy number estimation by using quantitative RT-PCR*

638 To estimate the number of plasmid fragments integrated into the genome via NHEJ events, we  
639 performed quantitative RT-PCR using total RNA from individual 5 day-old embryos of wild type,  
640 *Gb-Ubx*<sup>KI-exon</sup>, and *Gb-abd-A*<sup>KI-exon</sup> lines, and compared the level of expression of the inserted gene  
641 with that of *Gb-otd*, which is present in single copy in the *G. bimaculatus* genome (Nakamura et  
642 al., 2010; Ylla et al., 2021). Total RNA was extracted from embryos using ISOGEN (Nippon-Gene  
643 catalog #315-02504). After treatment with DNaseI (Invitrogen catalog #AM2224), RNA was  
644 reverse transcribed to cDNA using SuperScriptIII reverse transcriptase (Invitrogen catalog  
645 #12574026). Real-time quantitative PCR was performed using the power SYBR Green PCR  
646 Master Kit (Applied Biosystems catalogue #4368577) and an ABI 7900 Real Time PCR System  
647 (Applied Biosystems) as described previously (Nakamura et al., 2008). Primer sequences are listed  
648 in Table 4. The level of *eGFP* was normalized to the level of *Gb-otd*, which suggested that the *Gb-*  
649 *Ubx*<sup>KI-exon</sup> line likely contained four copies of the plasmid fragment, and *Gb-abd-A*<sup>KI-exon</sup> line likely  
650 contained a single copy of the plasmid fragment.

651 **Acknowledgements**

652 We thank N. Sakamoto for the Ars plasmid, and the members of the Extavour and Mito labs for  
653 discussion.

654

655 **Competing Interests**

656 No competing interests declared.

657

658 **Funding3)**

659 This work was supported by National Science Foundation award number IOS-1257217 and  
660 funds from Harvard University to CGE, an Overseas Research Fellowship (grant # 693) from the  
661 Japan Society for the Promotion of Science (JSPS) to TN, a Grant-in-Aid for Young Scientists B  
662 (grant # JP16K21199, JP26870415) from the JSPS to TW, and a Grant-in-Aid for Scientific  
663 Research (B) (grant # JP26292176) from the JSPS to TM.

664

665 **Data availability**

666 Not applicable.

667

668 **Figure Legends**

669

670 **Figure 1. *Gb-laccase2* knock-out G<sub>0</sub> and G<sub>1</sub> phenotypes.**

671 (A) Cuticle of adult wild type (WT) *G. bimaculatus* is uniformly dark brown or black. Head and  
672 anterior thorax shown in dorsal view. (A') *Gb-lac2* gene somatic mutagenesis in G<sub>0</sub> animals can  
673 be detected by the presence of white spots of cuticle (asterisks). (B) Representative cuticle  
674 phenotypes of G<sub>2</sub> homozygous mutant nymphs (B') at one day after hatching. Control first instar  
675 nymphs (B) have dark melanized cuticle by one day after hatching, while homozygous mutants  
676 (B') showed homogeneous pale brown cuticle even at one day after hatching. Scale bar: 1 mm. (C)  
677 T7 endonuclease I assay result. The control experiment, in which the PCR product was amplified  
678 from the genome of a wild type control individual, did not produce any band of the expected size  
679 after T7 endonuclease I treatment (white arrowhead). In contrast, the PCR product amplified from  
680 the genome of CRISPR reagent-injected animals included small fragments of the expected size  
681 after T7 endonuclease I treatment (black arrowhead). (D) Sequence analysis of *Gb-lac2* mutant  
682 alleles #6-2 and #1-10 induced by CRISPR/Cas9 system. Top row: wild-type sequences; green:  
683 Protospacer Adjacent Motif (PAM) sequence; red: target sequence; and arrowheads: predicted  
684 double strand break site. Asterisks at right show induced frame-shift mutations.

685

686 **Figure 2. Knock-out vs knock-down phenotype of *Gb-Ubx*.**

687 (A) Schematic diagram of *Ubx* locus. White boxes: exons; red box: homeodomain; black  
688 arrowhead: sgRNA target site. (B) Surveyor<sup>TM</sup> assay with G<sub>0</sub> eggs. Plus (+) indicates the PCR  
689 products digested by Surveyor<sup>TM</sup> nuclease; minus (-) indicates the PCR products with no digestion  
690 (no nuclease added). L = ladder. (C) Phenotype of heterozygous and homozygous *Gb-Ubx*<sup>CRISPR</sup>  
691 mutant stage X embryos. Anterior is to the left here and in all other figures. The size of the T3 leg  
692 (region between white arrowheads) was decreased mildly and severely in heterozygous and  
693 homozygous mutants, respectively. Anterior white arrowhead marks the posterior end of T3  
694 segment. Posterior white arrowhead marks the junction of femur and tibia. Asterisk indicates the  
695 A1 segment. (D) *Ubx*/*Abd-A* (*UbdA*) protein expression pattern in homozygous *Gb-Ubx*<sup>CRISPR</sup>  
696 stage X embryos and *Gb-Ubx*<sup>RNAi</sup> stage X embryos. In *Gb-Ubx*<sup>CRISPR</sup> embryos, only the T3/A1  
697 *Gb-Ubx* expression domain was undetectable. (E) In stage X *Gb-Ubx*<sup>RNAi</sup> embryos, *UbdA* protein  
698 expression was undetectable in the T3 leg (L3) but was still detected in the A1 segment. Scale bar:  
699 100 μm. Pp: pleuropodium. Embryonic staging as per (Donoughe and Extavour, 2016).

700  
701 **Figure 3. Exonic knock-in/Knock-out against *Gb-Ubx*.**  
702 (A) Scheme of knock-in experiment against *Gb-Ubx*. White box: exons; red box: homeodomain;  
703 black arrowhead: sgRNA target site. Donor vector contains bait sequence (yellow box) and  
704 expression cassette with the following elements: *Gryllus actin* promoter (blue arrow) followed by  
705 *eGFP* coding sequence (green box), and flanking *Ars* insulators (gray arrow). After co-injection  
706 of the donor vector with sgRNA for the donor vector, sgRNA for the genomic target site, and Cas9  
707 mRNA, two patterns of insertion are predicted to occur due to NHEJ. (B) GFP expression in *Gb-*  
708 *Ubx*<sup>KI</sup> G<sub>0</sub> and G<sub>1</sub> stage X embryos. 4.7% of G<sub>0</sub> embryos showed mosaic GFP expression in the T3  
709 legs (Table 3). In G<sub>1</sub> stage X embryos, the GFP expression pattern was identical to that of the  
710 previously reported expression pattern of *Gb-Ubx* (Barnett et al., 2019; Matsuoka et al., 2015;  
711 Zhang et al., 2005). (C) GFP expression in heterozygous and homozygous G<sub>2</sub> mutants. *Gb-Ubx*<sup>KI</sup>  
712 homozygous mutants showed strong GFP expression, and also showed phenotypes characteristic  
713 of *Gb-Ubx*<sup>CRISPR</sup> mutants, including shortened T3 legs and formation of leg-like structures on the  
714 A1 segment (FIG). Asterisks in (B) and (C) mark position of embryonic head. (D) Assessment of  
715 knock-in event by using PCR and Sanger sequencing. We designed PCR primers specific for each  
716 putative junction (black arrows flanking shaded areas in a and b of panel (A)), and all three G<sub>2</sub>  
717 individual mutant animals assayed showed bands of the expected size for each junction, suggesting  
718 that this *Gb-Ubx*<sup>KI</sup> line has at least two copies of donor vector insert. (E) Sequence analysis using  
719 the same primers indicated in (A) and (D) for genotyping confirmed that several deletions were  
720 generated due to the NHEJ events at each junction. Blue: genomic sequence; red: PAM sequence;  
721 pink: deleted nucleotides. Scale bar: 200 μm in (B) and (C). Embryonic staging as per (Donoughe  
722 and Extavour, 2016).

723  
724 **Figure 4. Exonic knock-in/Knock-out against *Gb-abd-A*.**

725 (A) Scheme of knock-in experiment against *Gb-abd-A*. White box: exons; red box: homeodomain;  
726 black arrowhead: sgRNA target site. We used the same donor vector construct as that used in the  
727 experiment against *Gb-Ubx* (Fig. 3), substituting a *Gb-abd-A* exon-specific sgRNA. Two patterns  
728 of insertion are predicted to occur due to NHEJ. (B) Expression of GFP in G<sub>0</sub> and G<sub>1</sub> *Gb-abd-A*<sup>KI</sup>  
729 embryos. 10.6% of G<sub>0</sub> *Gb-abd-A*<sup>KI</sup> embryos showed mosaic GFP expression in the abdomen of  
730 stage X embryos at seven days after injection (Table 3). In G<sub>1</sub> *Gb-abd-A*<sup>KI</sup> stage X embryos, the  
731 expression pattern of GFP was identical to the previously reported expression pattern of *Gb-abd-*



732 *A* (Barnett et al., 2019; Matsuoka et al., 2015; Zhang et al., 2005). (C) Assessment of knock-in  
733 event by using PCR and Sanger sequencing. Genomic DNA was extracted from the seven day G<sub>2</sub>  
734 *Gb-abd-A*<sup>KI</sup> stage X embryos and used as a PCR template. We designed PCR primers specific for  
735 each putative junction (black arrows and shaded regions a, b and c, d in panel (A)). The expected  
736 amplicon size was detected for each junction. (D) Sequence analysis using primers indicated in  
737 (A) and (C) for genotyping confirmed that multiple deletions or insertions were generated due to the  
738 NHEJ events at each junction. Blue: genomic sequence; red: PAM sequence; pink: deleted or  
739 inserted nucleotides. Scale bar: 200 μm in (B) and (C). Embryonic staging as per (Donoughe and  
740 Extavour, 2016).

741

#### 742 **Figure 5. Intronic knock-in against *Gb-abd-A*.**

743 (A) Scheme of knock-in experiment targeted to a *Gb-abd-A* intron. White boxes: exons; red box:  
744 homeodomain; black arrowhead: sgRNA target site. We used the same donor vector construct as  
745 that used in the experiment against *Gb-Ubx* (Fig. 3), substituting a *Gb-abd-A* intron-specific  
746 sgRNA. Two patterns of insertion are predicted to occur due to NHEJ. (B) Expression pattern of  
747 GFP in G<sub>0</sub> and G<sub>2</sub> stage X KI embryonic abdomen. In *Gb-abd-A*<sup>KI-exon</sup> embryos, patchy GFP  
748 expression was accompanied by ectopic phenotypic leg-like structures (arrowheads; compare with  
749 Fig.4B). In *Gb-abd-A*<sup>KI-intron</sup> embryos, patchy GFP expression was observed but embryos did not  
750 show the ectopic abdominal appendage phenotype of *Gb-abd-A*<sup>KI-exon</sup> embryos. *Gb-abd-A*<sup>KI-intron</sup>  
751 G<sub>2</sub> heterozygous embryos show abdominal GFP expression corresponding to the known pattern of  
752 embryonic *Gb-abd-A* transcripts (Barnett et al., 2019; Matsuoka et al., 2015; Zhang et al., 2005),  
753 and the embryos did not show any morphological abnormality. *Gb-abd-A*<sup>KI-intron</sup> G<sub>2</sub> homozygous  
754 embryos generated ectopic leg-like structures on the abdomen (white arrowheads) as observed in  
755 G<sub>0</sub> *Gb-abd-A*<sup>CRISPR</sup> embryos (compare with (B')). Scale bar: 500 μm. Embryonic staging as per  
756 (Donoughe and Extavour, 2016).

757

## Tables

Table 1. *G. bimaculatus* genes disrupted by targeted genome modification

<i>Gene</i>	<i>Functions</i>	<i>Tissue distribution</i>	<i>Phenotype of Knockout/Knockdown cricket</i>	<i>Refs</i>
<i>Laccase 2</i>	Phenol oxidase, cuticle tuning (sclerotization and pigmentation)	ND	<i>Lac2</i> knock-out nymphs show defect in pigmentation.	(Watanabe et al., 2014); this study
<i>Ultrabithorax</i>	Enlargement of T3 leg Identification of A1 pleuropodia	T3 and A1 segment	- <i>Ubx</i> knock-out embryos show partial transformation of A1 pleuropodia into T3 thoracic leg, and of T3 thoracic leg into T2 thoracic leg. - Embryonic lethal.	This study
<i>abdominal-A</i>	Repression of leg formation in abdomen	Abdomen	- <i>abd-A</i> knock-out embryos show generation of leg-like structures on the abdomen. - <i>abd-A</i> knock-out nymphs show fusion of abdominal segments. - <i>abd-A</i> knock-out female adults generated ectopic ovipositors and had defects in oviducts and uterus attachment.	This study

**Table 2. sgRNA sequences used in this study**

<i>sgRNA name</i>	<i>sgRNA sequence (5'-&gt;3') (<b><u>Bold underline</u></b> indicates PAM sequence)</i>
<i>Gb-lac2</i> exon	GGGGTCCTGGCCCGGGTTGAC <b><u>CGG</u></b>
<i>Gb-Ubx</i> exon	GGGTAGAAGGTGTGGTTGGC <b><u>GGG</u></b>
<i>Gb-Ubx</i> intron	GGACTGGCCACGCTCCAAGG <b><u>AGG</u></b>
<i>Gb-abd-A</i> exon	GGGGCAAGGCTCACCCGTGAT <b><u>TGG</u></b>
<i>Gb-abd-A</i> intron	GCTCGCGGTGTTTTACGGCT <b><u>GGG</u></b>

**Table 3. Efficiency of CRISPR/Cas9-mediated genome editing in *G. bimaculatus***

	<i>Shown in Figure</i>	<i># eggs injected</i>	<i># injected embryos with GFP expression or phenotype</i>	<i># embryos developed by 7d AEL (% of injected embryos)</i>	<i># hatched nymphs (% of embryos developed by 7d AEL)</i>	<i># fertile adults (% of nymphs hatched)</i>	<i>% injected embryos yielding fertile adults</i>	<i># fertile adults showing germ line transmission</i>	<i>% fertile adults showing germ line transmission</i>	<i>% injected embryos yielding fertile adults showing germline transmission</i>
<i>Gb-Lac2<sup>CRISPR</sup></i> KO	1	128	nd	nd	nd	18 (nd)	14.1%	14	77.8%	10.9%
<i>Gb-Ubx<sup>CRISPR</sup></i> KO	2, S1, S2	167	nd	nd	nd	10 (nd)	59.9%	6	60.0%	3.6%
<i>Gb-Ubx<sup>KI</sup></i> exon	3, S3, S4	85	4 (4.7%)	58 (68.2%)	30 (51.7%)	25 (83.3%)	29.4%	1	4.0%	1.2%
<i>Gb-abd-A<sup>KI</sup></i> exon <i>1<sup>st</sup> trial</i>	4, S2, S3, S4, S5, S6	47	5 (10.6%)	38 (80.8%)	9 (23.7%)	4 (44.4%)	8.5%	1	25.0%	2.1%
<i>Gb-abd-A<sup>KI</sup></i> exon <i>2<sup>nd</sup> trial</i>	n/a	41	0 (0.0%)	36 (87.8%)	22 (61.1%)	2 (9.1%)	4.9%	1	50.0%	2.4%
<i>Gb-abd-A<sup>KI</sup></i> intron	5, S5, S6	100	2 (2.0%)	77 (77.0%)	47 (61.0%)	28 (59.6%)	28.0%	1	3.6%	1.0%
<i>Gb-Ubx KI</i> intron	S7	73	5 (6.8%)	62 (84.9%)	59 (95.2%)	22 (37.3%)	30.1%	2	9.1%	2.7%

Control	n/a	42	40 (95.2%)	28 (70.0%)
---------	-----	----	------------	------------

(Donoughe  
and Extavour,  
2016)

Control	n/a	78	64 (82.0%)
---------	-----	----	------------

(Ewen-  
Campen et  
al., 2012)

1 **Table 4. Primers used in this study.**

2

<i>Primer name</i>	<i>Primer seq (5'→3')</i>
<i>Gb-Ubx</i> exon genotype KO Fw	CGTTTGTGAAACGTATGGCCCGTTA
<i>Gb-Ubx</i> exon genotype KO Rv	GTCCCTGGGCTCCTGGAACACG
<i>Gb-Ubx</i> exon genotype KI genome Fw	AACACGTGCTCCCTCAACTC
<i>Gb-Ubx</i> exon genotype KI genome Rv	TGAAACGTATGGCCCGTTAT
<i>Gb-Ubx</i> exon genotype KI vector 5' Rv	GTCGCATGCTCCTCTAGACTCG
<i>Gb-Ubx</i> intron genotype Fw	GCAGAACCGTTTCATGAATGT
<i>Gb-Ubx</i> intron genotype Rv	ATTCTCGCCCTTATGCAGAG
<i>Gb-abd-A</i> exon genotype Fw	CCGATTCCATGGTGAACTA
<i>Gb-abd-A</i> exon genotype Rv	AGAACGGAACGCAGTGAGTTAG
<i>Gb-abd-A</i> exon genotype vector 3'	GAACTTCAGGGTCAGCTTGC
<i>Gb-abd-A</i> exon genotype vector 5'	CACAAGGCACAAATGCTCGT
<i>Gb-abd-A</i> intron Fw	CGGATCTATTCGGCCATT
<i>Gb-abd-A</i> intron Rv	TCAAACGGATCTTCCTCTCG
<i>Gb-otd</i> qPCR Fw	CATTCACGTCTCCGCCATAC
<i>Gb-otd</i> qPCR Rv	GCTCCATCAACAGGCAAACA
<i>eGFP</i> qPCR Fw	CAGAAGAACGGCATCAAGGT
<i>eGFP</i> qPCR Rv	GGGTGCTCAGGTAGTGGTTG

3

4

5 **References**

6

7

8 **Amitai, G. and Sorek, R.** (2016). CRISPR–Cas adaptation: insights into the mechanism of  
9 action. *Nat Rev Microbiol* **14**, 67–76.

10 **Arakane, Y., Muthukrishnan, S., Beeman, R. W., Kanost, M. R. and Kramer, K. J.** (2005).  
11 Laccase 2 is the phenoloxidase gene required for beetle cuticle tanning. *P Natl Acad Sci Usa*  
12 **102**, 11337–11342.

13 **Ashburner, M., Ball, C. A., Blake, J. A., Botstein, D., Butler, H., Cherry, J. M., Davis, A. P.,**  
14 **Dolinski, K., Dwight, S. S., Eppig, J. T., et al.** (2000). Gene Ontology: tool for the  
15 unification of biology. *Nat Genet* **25**, 25–29.

16 **Auer, T. O., Durore, K., Cian, A. D., Concordet, J.-P. and Bene, F. D.** (2014). Highly  
17 efficient CRISPR/Cas9-mediated knock-in in zebrafish by homology-independent DNA  
18 repair. *Genome Res* **24**, 142–153.

19 **Baird, G. S., Zacharias, D. A. and Tsien, R. Y.** (2000). Biochemistry, mutagenesis, and  
20 oligomerization of DsRed, a red fluorescent protein from coral. *Proc National Acad Sci* **97**,  
21 11984–11989.

22 **Bando, T., Ishimaru, Y., Kida, T., Hamada, Y., Matsuoka, Y., Nakamura, T., Ohuchi, H.,**  
23 **Noji, S. and Mito, T.** (2013). Analysis of RNA-Seq data reveals involvement of JAK/STAT  
24 signalling during leg regeneration in the cricket *Gryllus bimaculatus*. *Development* **140**, 959–  
25 964.

26 **Barnett, A. A., Nakamura, T. and Extavour, C. G.** (2019). Hox genes limit germ cell  
27 formation in the short germ insect *Gryllus bimaculatus*. *Proc National Acad Sci* **116**, 16430–  
28 16435.

29 **Barry, S. K., Nakamura, T., Matsuoka, Y., Straub, C., Horch, H. W. and Extavour, C. G.**  
30 (2019). Injecting *Gryllus bimaculatus* Eggs. *J Vis Exp*.

- 31 **Bosch, J. A., Colbeth, R., Zirin, J. and Perrimon, N.** (2019). Gene Knock-Ins in *Drosophila*  
32 Using Homology-Independent Insertion of Universal Donor Plasmids. *Genetics* **214**,  
33 genetics.302819.2019.
- 34 **Branzei, D. and Foiani, M.** (2008). Regulation of DNA repair throughout the cell cycle. *Nat*  
35 *Rev Mol Cell Bio* **9**, 297–308.
- 36 **Brown, J. B., Boley, N., Eisman, R., May, G. E., Stoiber, M. H., Duff, M. O., Booth, B. W.,**  
37 **Wen, J., Park, S., Suzuki, A. M., et al.** (2014). Diversity and dynamics of the *Drosophila*  
38 transcriptome. *Nature* **512**, 393–399.
- 39 **Carballar-Lejarazú, R., Jasinskiene, N. and James, A. A.** (2013). Exogenous gypsy insulator  
40 sequences modulate transgene expression in the malaria vector mosquito, *Anopheles*  
41 *stephensi*. *Proc National Acad Sci* **110**, 7176–7181.
- 42 **Consortium, T. G. O., Carbon, S., Douglass, E., Good, B. M., Unni, D. R., Harris, N. L.,**  
43 **Mungall, C. J., Basu, S., Chisholm, R. L., Dodson, R. J., et al.** (2020). The Gene Ontology  
44 resource: enriching a GOld mine. *Nucleic Acids Res* **49**, D325–D334.
- 45 **Dabour, N., Bando, T., Nakamura, T., Miyawaki, K., Mito, T., Ohuchi, H. and Noji, S.**  
46 (2011). Cricket body size is altered by systemic RNAi against insulin signaling components  
47 and epidermal growth factor receptor. *Dev Growth Differ* **53**, 857–869.
- 48 **Daimon, T., Uchibori, M., Nakao, H., Sezutsu, H. and Shinoda, T.** (2015). Knockout  
49 silkworms reveal a dispensable role for juvenile hormones in holometabolous life cycle. *Proc*  
50 *National Acad Sci* **112**, E4226–E4235.
- 51 **Davis, G. K. and Patel, N. H.** (2002). SHORT, LONG, AND BEYOND: Molecular and  
52 Embryological Approaches to Insect Segmentation. *Annual Review of Entomology* **47**, 669–  
53 699.
- 54 **Donoughe, S. and Extavour, C. G.** (2016). Embryonic development of the cricket *Gryllus*  
55 *bimaculatus*. *Dev Biol* **411**, 140–156.



- 56 **Donoughe, S., Nakamura, T., Ewen-Campen, B., Green, D. A., Henderson, L. and**  
57 **Extavour, C. G.** (2014). BMP signaling is required for the generation of primordial germ  
58 cells in an insect. *Proc National Acad Sci* **111**, 4133–4138.
- 59 **Epper, F.** (1983). The evagination of the genital imaginal discs of *Drosophila melanogaster*.  
60 *Wilhelm Roux's Archives Dev Biology* **192**, 275–279.
- 61 **Ewen-Campen, B., Srouji, J. R., Schwager, E. E. and Extavour, C. G.** (2012). oskar Predates  
62 the Evolution of Germ Plasm in Insects. *Curr Biol* **22**, 2278–2283.
- 63 **Foe, V. E. and Alberts, B. M.** (1983). Studies of nuclear and cytoplasmic behaviour during the  
64 five mitotic cycles that precede gastrulation in *Drosophila* embryogenesis. *Journal of Cell*  
65 *Science* **61**, 31–70.
- 66 **Foronda, D., Estrada, B., Navas, L. de and Sánchez-Herrero, E.** (2006). Requirement of  
67 abdominal-A and Abdominal-B in the developing genitalia of *Drosophila* breaks the posterior  
68 downregulation rule. *Development* **133**, 117–127.
- 69 **Freeland, D. E. and Kuhn, D. T.** (1996). Expression patterns of developmental genes reveal  
70 segment and parasegment organization of *D. melanogaster* genital discs. *Mech Develop* **56**,  
71 61–72.
- 72 **Gilles, A. F., Schinko, J. B. and Averof, M.** (2015). Efficient CRISPR-mediated gene targeting  
73 and transgene replacement in the beetle *Tribolium castaneum*. *Development* **142**, 2832–2839.
- 74 **Goldstein, B. and King, N.** (2016). The Future of Cell Biology: Emerging Model Organisms.  
75 *Trends Cell Biol* **26**, 818–824.
- 76 **Gratz, S. J., Cummings, A. M., Nguyen, J. N., Hamm, D. C., Donohue, L. K., Harrison, M.**  
77 **M., Wildonger, J. and O'Connor-Giles, K. M.** (2013). Genome Engineering of *Drosophila*  
78 with the CRISPR RNA-Guided Cas9 Nuclease. *Genetics* **194**, 1029–1035.
- 79 **Hagmann, M., Bruggmann, R., Xue, L., Georgiev, O., Schaffner, W., Rungger, D., Spaniol,**  
80 **P. and Gerster, T.** (1998). Homologous Recombination and DNA-End Joining Reactions in

- 81 Zygotes and Early Embryos of Zebrafish (*Danio rerio*) and *Drosophila melanogaster*. *Biol*  
82 *Chem* **379**, 673–682.
- 83 **Hedwig, B. and Sarmiento-Ponce, E. J.** (2017). Song pattern recognition in crickets based on a  
84 delay-line and coincidence-detector mechanism. *Proc Royal Soc B* **284**, 20170745.
- 85 **Hendel, A., Bak, R. O., Clark, J. T., Kennedy, A. B., Ryan, D. E., Roy, S., Steinfeld, I.,**  
86 **Lunstad, B. D., Kaiser, R. J., Wilkens, A. B., et al.** (2015). Chemically modified guide  
87 RNAs enhance CRISPR-Cas genome editing in human primary cells. *Nat Biotechnol* **33**,  
88 985–989.
- 89 **Horch, H. Wi., Mito, T., Popadic, A., Ohuchi, H. and Noji, S.** (2017a). *The Cricket as a*  
90 *Model Organism, Development, Regeneration, and Behavior*.
- 91 **Horch, H., Liu, J., Mito, T., Popadić, A. and Watanabe, T.** (2017b). Protocols in the Cricket.  
92 In *The Cricket as a Model Organism* (ed. Horch, H.), Mito, T.), Popadic, A.), Hideyo),  
93 Ohuchi), and Noji, S.), pp. 327–370.
- 94 **Hsu, P. D., Scott, D. A., Weinstein, J. A., Ran, F. A., Konermann, S., Agarwala, V., Li, Y.,**  
95 **Fine, E. J., Wu, X., Shalem, O., et al.** (2013). DNA targeting specificity of RNA-guided  
96 Cas9 nucleases. *Nat Biotechnol* **31**, 827–832.
- 97 **Huis, A. van, Itterbeeck, J. V., Klunder, H., Mertens, E., Halloran, A., Muir, G. and**  
98 **Vantomme, P.** (2013). *Edible insects: Future prospects for food and feed security*. Rome:  
99 Food and Agriculture Organization of the United Nations.
- 100 **Jinek, M., Chylinski, K., Fonfara, I., Hauer, M., Doudna, J. A. and Charpentier, E.** (2012).  
101 A Programmable Dual-RNA-Guided DNA Endonuclease in Adaptive Bacterial Immunity.  
102 *Science* **337**, 816–821.
- 103 **Kelsh, R., Weinzierl, R. O. J., White, R. A. H. and Akam, M.** (1994). Homeotic gene  
104 expression in the locust *Schistocerca*: An antibody that detects conserved epitopes in  
105 ultrabithorax and abdominal-A proteins. *Dev Genet* **15**, 19–31.

- 106 **Kimura, Y., Hisano, Y., Kawahara, A. and Higashijima, S.** (2014). Efficient generation of  
107 knock-in transgenic zebrafish carrying reporter/driver genes by CRISPR/Cas9-mediated  
108 genome engineering. *Sci Rep-uk* **4**, 6545.
- 109 **Kistler, K. E., Vosshall, L. B. and Matthews, B. J.** (2015). Genome Engineering with  
110 CRISPR-Cas9 in the Mosquito *Aedes aegypti*. *Cell Reports* **11**, 51–60.
- 111 **Kulkarni, A. and Extavour, C. G.** (2019). Chapter 8: The Cricket *Gryllus bimaculatus*:  
112 Techniques for Quantitative and Functional Genetic Analyses of Cricket Biology. In *Evo-  
113 Devo: Non-model Species in Cell and Developmental Biology* (ed. Twozydlo, W.) and  
114 Bilinski, S. M.), pp. 183–216.
- 115 **Kulski, J. K.** (2016). Next Generation Sequencing - Advances, Applications and Challenges.
- 116 **Li, X., Fan, D., Zhang, W., Liu, G., Zhang, L., Zhao, L., Fang, X., Chen, L., Dong, Y.,  
117 Chen, Y., et al.** (2015). Outbred genome sequencing and CRISPR/Cas9 gene editing in  
118 butterflies. *Nat Commun* **6**, 8212.
- 119 **Ma, S., Chang, J., Wang, X., Liu, Y., Zhang, J., Lu, W., Gao, J., Shi, R., Zhao, P. and Xia,  
120 Q.** (2014). CRISPR/Cas9 mediated multiplex genome editing and heritable mutagenesis of  
121 BmKu70 in *Bombyx mori*. *Sci Rep-uk* **4**, 4489.
- 122 **Mahfooz, N. S., Li, H. and Popadić, A.** (2004). Differential expression patterns of the hox gene  
123 are associated with differential growth of insect hind legs. *P Natl Acad Sci Usa* **101**, 4877–  
124 4882.
- 125 **Mahfooz, N., Turchyn, N., Mihajlovic, M., Hrycaj, S. and Popadić, A.** (2007). Ubx Regulates  
126 Differential Enlargement and Diversification of Insect Hind Legs. *Plos One* **2**, e866.
- 127 **Martin, A., Serano, J. M., Jarvis, E., Bruce, H. S., Wang, J., Ray, S., Barker, C. A.,  
128 O’Connell, L. C. and Patel, N. H.** (2016). CRISPR/Cas9 Mutagenesis Reveals Versatile  
129 Roles of Hox Genes in Crustacean Limb Specification and Evolution. *Curr Biol* **26**, 14–26.
- 130 **Matsumoto, Y., Matsumoto, C. S. and Mizunami, M.** (2018). Signaling Pathways for Long-  
131 Term Memory Formation in the Cricket. *Front Psychol* **9**, 1014.

- 132 **Matsuoka, Y. and Monteiro, A.** (2018). Melanin Pathway Genes Regulate Color and  
133 Morphology of Butterfly Wing Scales. *Cell Reports* **24**, 56–65.
- 134 **Matsuoka, Y., Bando, T., Watanabe, T., Ishimaru, Y., Noji, S., Popadić, A. and Mito, T.**  
135 (2015). Short germ insects utilize both the ancestral and derived mode of Polycomb group-  
136 mediated epigenetic silencing of Hox genes. *Biol Open* **4**, 702–709.
- 137 **McMeniman, C. J., Corfas, R. A., Matthews, B. J., Ritchie, S. A. and Vosshall, L. B.** (2014).  
138 Multimodal Integration of Carbon Dioxide and Other Sensory Cues Drives Mosquito  
139 Attraction to Humans. *Cell* **156**, 1060–1071.
- 140 **Miller, D. E., Cook, K. R. and Hawley, R. S.** (2019). The joy of balancers. *Plos Genet* **15**,  
141 e1008421.
- 142 **Minelli, A.** (2016). Evo-Devo and Phylogenetics. In *Evolutionary Developmental Biology*, pp.  
143 1–12.
- 144 **Mito, T. and Noji, S.** (2008). The Two-Spotted Cricket *Gryllus bimaculatus*: An Emerging  
145 Model for Developmental and Regeneration Studies. *Cold Spring Harb Protoc* **2008**,  
146 pdb.emo110-pdb.emo110.
- 147 **Mito, T., Inoue, Y., Kimura, S., Miyawaki, K., Niwa, N., Shinmyo, Y., Ohuchi, H. and Noji,**  
148 **S.** (2002). Involvement of hedgehog, wingless, and dpp in the initiation of proximodistal axis  
149 formation during the regeneration of insect legs, a verification of the modified boundary  
150 model. *Mech Develop* **114**, 27–35.
- 151 **Mito, T., Kobayashi, C., Sarashina, I., Zhang, H., Shinahara, W., Miyawaki, K., Shinmyo,**  
152 **Y., Ohuchi, H. and Noji, S.** (2007). even-skipped has gap-like, pair-rule-like, and segmental  
153 functions in the cricket *Gryllus bimaculatus*, a basal, intermediate germ insect (Orthoptera).  
154 *Dev Biol* **303**, 202–213.
- 155 **Mito, T., Ronco, M., Uda, T., Nakamura, T., Ohuchi, H. and Noji, S.** (2008). Divergent and  
156 conserved roles of extradenticle in body segmentation and appendage formation, respectively,  
157 in the cricket *Gryllus bimaculatus*. *Dev Biol* **313**, 67–79.

- 158 **Mizunami, M. and Matsumoto, Y.** (2017). Roles of Octopamine and Dopamine Neurons for  
159 Mediating Appetitive and Aversive Signals in Pavlovian Conditioning in Crickets. *Front*  
160 *Physiol* **8**, 1027.
- 161 **Modolell, J., Bender, W. and Meselson, M.** (1983). *Drosophila melanogaster* mutations  
162 suppressible by the suppressor of Hairy-wing are insertions of a 7.3-kilobase mobile element.  
163 *Proc National Acad Sci* **80**, 1678–1682.
- 164 **Nakamura, T., Mito, T., Bando, T., Ohuchi, H. and Noji, S.** (2007). Molecular and Cellular  
165 Basis of Regeneration and Tissue Repair. *Cell Mol Life Sci* **65**, 64.
- 166 **Nakamura, T., Mito, T., Miyawaki, K., Ohuchi, H. and Noji, S.** (2008). EGFR signaling is  
167 required for re-establishing the proximodistal axis during distal leg regeneration in the cricket  
168 *Gryllus bimaculatus* nymph. *Dev Biol* **319**, 46–55.
- 169 **Nakamura, T., Yoshizaki, M., Ogawa, S., Okamoto, H., Shinmyo, Y., Bando, T., Ohuchi,**  
170 **H., Noji, S. and Mito, T.** (2010). Imaging of Transgenic Cricket Embryos Reveals Cell  
171 Movements Consistent with a Syncytial Patterning Mechanism. *Curr Biol* **20**, 1641–1647.
- 172 **Nandchahal, N.** (1972). Reproductive organs of *Gryllodes sigillatus* (Walker) (Orthoptera:  
173 Gryllidae). *J Nat Hist* **6**, 125–131.
- 174 **Niwa, N., Inoue, Y., Nozawa, A., Saito, M., Misumi, Y., Ohuchi, H., Yoshioka, H. and Noji,**  
175 **S.** (2000). Correlation of diversity of leg morphology in *Gryllus bimaculatus* (cricket) with  
176 divergence in *dpp* expression pattern during leg development. *Development* **127**, 4373–4381.
- 177 **Papageorgiou, L., Eleni, P., Raftopoulou, S., Mantaïou, M., Megalooikonomou, V. and**  
178 **Vlachakis, D.** (2018). Genomic big data hitting the storage bottleneck. *Embnet J* **24**, e910.
- 179 **Pinello, L., Canver, M. C., Hoban, M. D., Orkin, S. H., Kohn, D. B., Bauer, D. E. and Yuan,**  
180 **G.-C.** (2016). Analyzing CRISPR genome-editing experiments with CRISPResso. *Nat*  
181 *Biotechnol* **34**, 695–697.
- 182 **Qiu, P., Shandilya, H., D’Alessio, J. M., O’Connor, K., Durocher, J. and Gerard, G. F.**  
183 (2004). Mutation detection using Surveyor nuclease. *Biotechniques* **36**, 702–707.

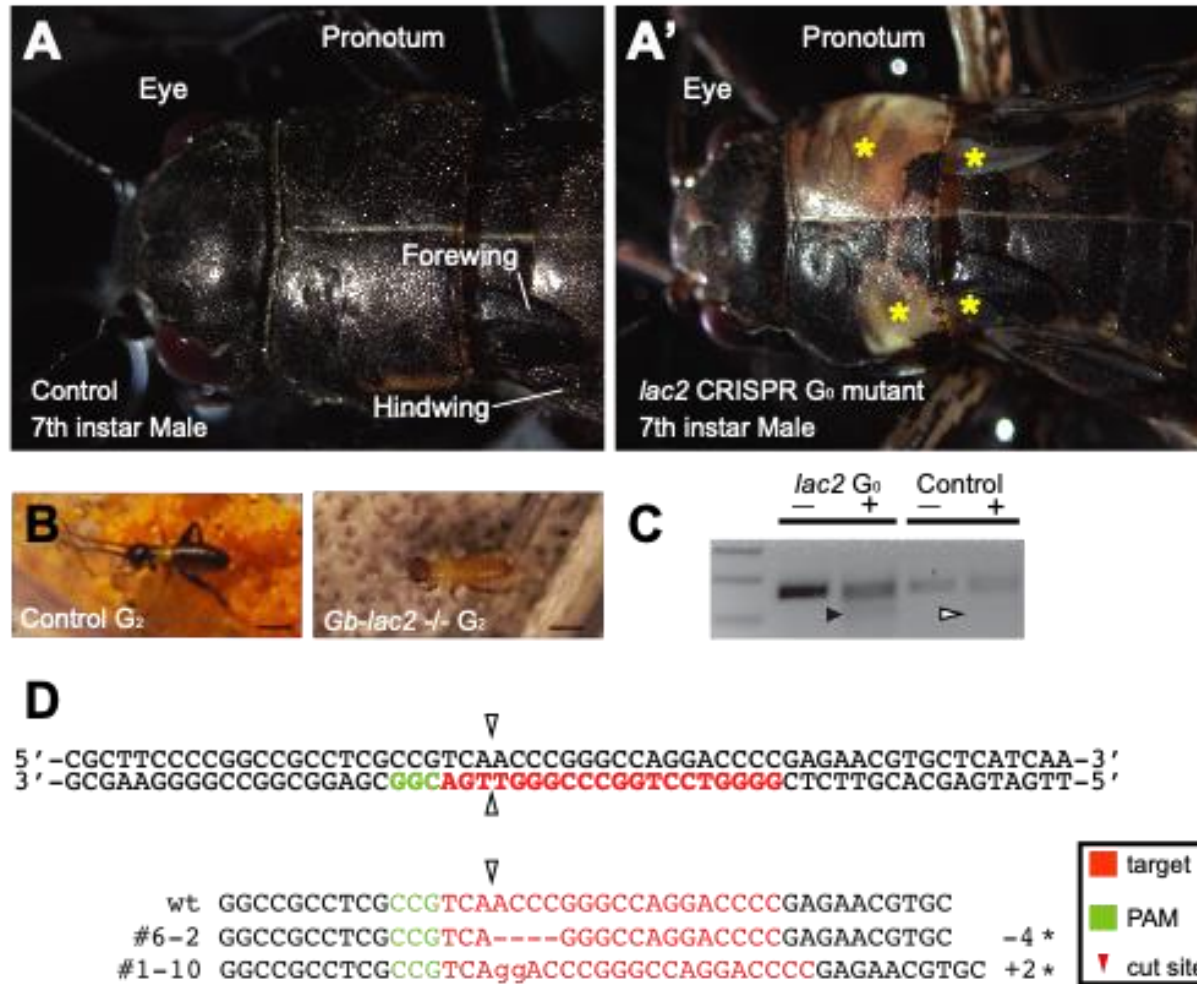
- 184 **Rathke, H.** (1844). Entwicklungsgeschichte der Maulwurfsgrille (*Gryllotalpa vulgaris*). *Archiv*  
185 *für Anatomie, Physiologie und Wissenschaftliche Medizin* 27–37.
- 186 **Ren, X., Yang, Z., Xu, J., Sun, J., Mao, D., Hu, Y., Yang, S.-J., Qiao, H.-H., Wang, X., Hu,**  
187 **Q., et al.** (2014). Enhanced Specificity and Efficiency of the CRISPR/Cas9 System with  
188 Optimized sgRNA Parameters in *Drosophila*. *Cell Reports* **9**, 1151–1162.
- 189 **Russell, J. J., Theriot, J. A., Sood, P., Marshall, W. F., Landweber, L. F., Fritz-Laylin, L.,**  
190 **Polka, J. K., Oliferenko, S., Gerbich, T., Gladfelter, A., et al.** (2017). Non-model model  
191 organisms. *Bmc Biol* **15**, 55.
- 192 **Sánchez, L. and Guerrero, I.** (2001). The development of the *Drosophila* genital disc.  
193 *Bioessays* **23**, 698–707.
- 194 **Sander, J. D., Zaback, P., Joung, J. K., Voytas, D. F. and Dobbs, D.** (2007). Zinc Finger  
195 Targeter (ZiFiT): an engineered zinc finger/target site design tool. *Nucleic Acids Res* **35**,  
196 W599–W605.
- 197 **Sander, J. D., Maeder, M. L., Reyon, D., Voytas, D. F., Joung, J. K. and Dobbs, D.** (2010).  
198 ZiFiT (Zinc Finger Targeter): an updated zinc finger engineering tool. *Nucleic Acids Res* **38**,  
199 W462–W468.
- 200 **Sarashina, I., Shinmyo, Y., Hirose, A., Miyawaki, K., Mito, T., Ohuchi, H., Horio, T. and**  
201 **Noji, S.** (2003). Hypotonic buffer induces meiosis and formation of anucleate cytoplasmic  
202 islands in the egg of the two-spotted cricket *Gryllus bimaculatus*. *Dev Growth Differ* **45**, 103–  
203 112.
- 204 **Takagi, H., Inai, Y., Watanabe, S. -i, Tatemoto, S., Yajima, M., Akasaka, K., Yamamoto, T.**  
205 **and Sakamoto, N.** (2011). Nucleosome exclusion from the interspecies-conserved central  
206 AT-rich region of the *Ars* insulator. *J Biochem* **151**, 75–87.
- 207 **Takahashi, T., Hamada, A., Miyawaki, K., Matsumoto, Y., Mito, T., Noji, S. and**  
208 **Mizunami, M.** (2009). Systemic RNA interference for the study of learning and memory in  
209 an insect. *J Neurosci Meth* **179**, 9–15.

- 210 **Tchurikov, N. A., Kretova, O. V., Moiseeva, E. D. and Sosin, D. V.** (2009). Evidence for  
211 RNA synthesis in the intergenic region between enhancer and promoter and its inhibition by  
212 insulators in *Drosophila melanogaster*. *Nucleic Acids Res* **37**, 111–122.
- 213 **Thorvaldsdóttir, H., Robinson, J. T. and Mesirov, J. P.** (2013). Integrative Genomics Viewer  
214 (IGV): high-performance genomics data visualization and exploration. *Brief Bioinform* **14**,  
215 178–192.
- 216 **Tomiya, Y., Shinohara, T., Matsuka, M., Bando, T., Mito, T. and Tomioka, K.** (2020).  
217 The role of clockwork orange in the circadian clock of the cricket *Gryllus bimaculatus*.  
218 *Zoological Lett* **6**, 12.
- 219 **Wainberg, M., Kamber, R. A., Balsubramani, A., Meyers, R. M., Sinnott-Armstrong, N.,**  
220 **Hornburg, D., Jiang, L., Chan, J., Jian, R., Gu, M., et al.** (2021). A genome-wide atlas of  
221 co-essential modules assigns function to uncharacterized genes. *Nat Genet* 1–12.
- 222 **Watanabe, T., Ochiai, H., Sakuma, T., Horch, H. W., Hamaguchi, N., Nakamura, T.,**  
223 **Bando, T., Ohuchi, H., Yamamoto, T., Noji, S., et al.** (2012). Non-transgenic genome  
224 modifications in a hemimetabolous insect using zinc-finger and TAL effector nucleases. *Nat*  
225 *Commun* **3**, 1017.
- 226 **Watanabe, T., Noji, S. and Mito, T.** (2014). Gene knockout by targeted mutagenesis in a  
227 hemimetabolous insect, the two-spotted cricket *Gryllus bimaculatus*, using TALENs. *Methods*  
228 **69**, 17–21.
- 229 **Watanabe, T., Noji, S. and Mito, T.** (2017). Genome Editing in Animals, Methods and  
230 Protocols. *Methods Mol Biology* **1630**, 219–233.
- 231 **Wheeler, W. M.** (1892). On the appendages of the first abdominal segment of embryo insects.  
232 *Transactions of the Wisconsin Academy of Sciences, Arts and Letters* **8**, 87–140.
- 233 **Xiao, A., Cheng, Z., Kong, L., Zhu, Z., Lin, S., Gao, G. and Zhang, B.** (2014). CasOT: a  
234 genome-wide Cas9/gRNA off-target searching tool. *Bioinformatics* **30**, 1180–1182.

- 235 **Ylla, G., Nakamura, T., Itoh, T., Kajitani, R., Toyoda, A., Tomonari, S., Bando, T.,**  
236 **Ishimaru, Y., Watanabe, T., Fuketa, M., et al.** (2021). Insights into the genomic evolution  
237 of insects from cricket genomes. *Communications Biology* in press,.
- 238 **Yoshimi, K., Kunihiro, Y., Kaneko, T., Nagahora, H., Voigt, B. and Mashimo, T.** (2016).  
239 ssODN-mediated knock-in with CRISPR-Cas for large genomic regions in zygotes. *Nat*  
240 *Commun* **7**, 10431.
- 241 **Zhang, H., Shinmyo, Y., Mito, T., Miyawaki, K., Sarashina, I., Ohuchi, H. and Noji, S.**  
242 (2005). Expression patterns of the homeotic genes *Scr*, *Antp*, *Ubx*, and *abd-A* during  
243 embryogenesis of the cricket *Gryllus bimaculatus*. *Gene Expr Patterns* **5**, 491–502.
- 244 **Zhang, L., Martin, A., Perry, M. W., Burg, K. R. L. van der, Matsuoka, Y., Monteiro, A.**  
245 **and Reed, R. D.** (2017). Genetic Basis of Melanin Pigmentation in Butterfly Wings. *Genetics*  
246 **205**, 1537–1550.
- 247 **Zhu, L., Mon, H., Xu, J., Lee, J. M. and Kusakabe, T.** (2015). CRISPR/Cas9-mediated  
248 knockout of factors in non-homologous end joining pathway enhances gene targeting in  
249 silkworm cells. *Sci Rep-uk* **5**, 18103.
- 250



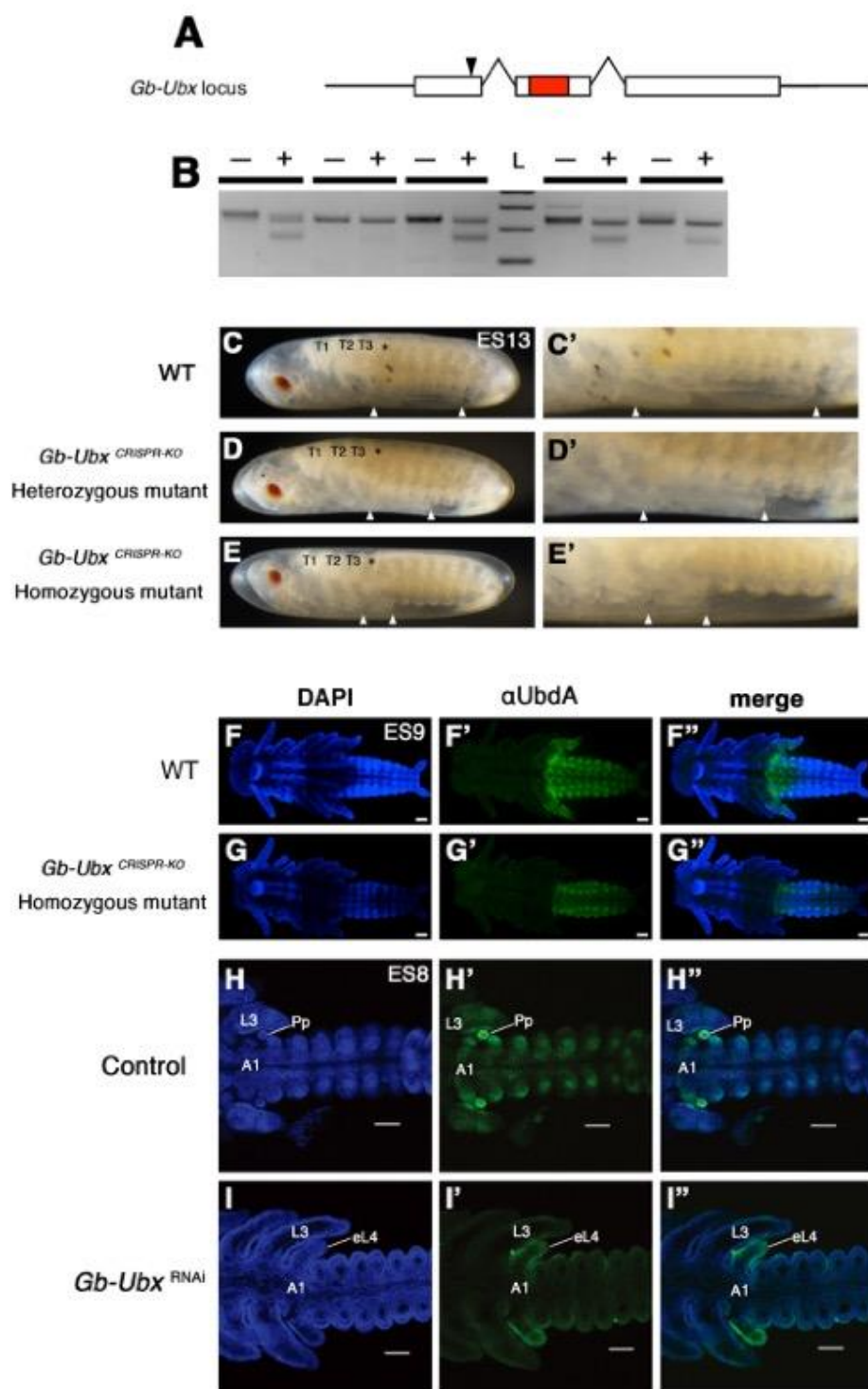
251 **Figure 1**



252

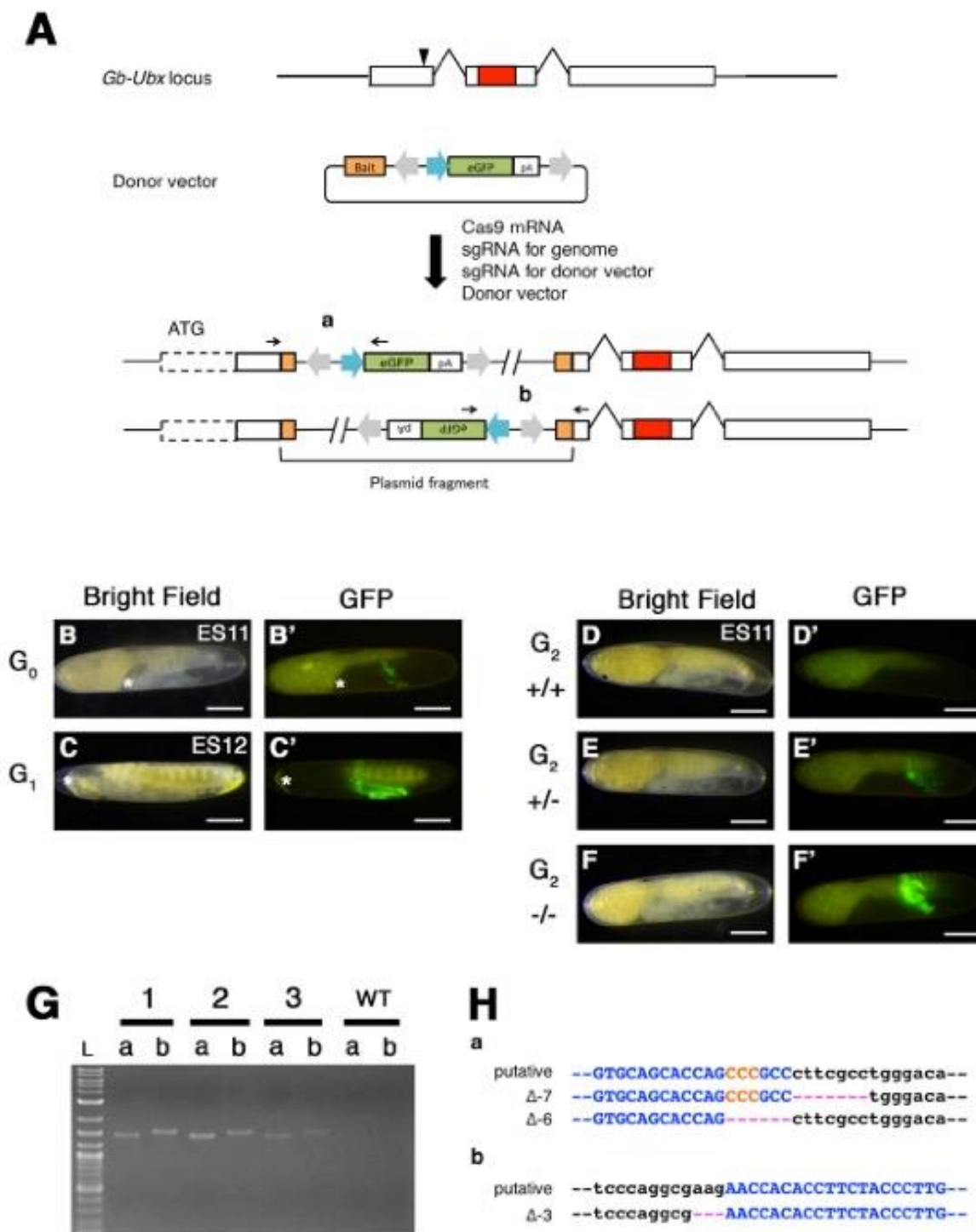
253 **Figure 2**

254



255

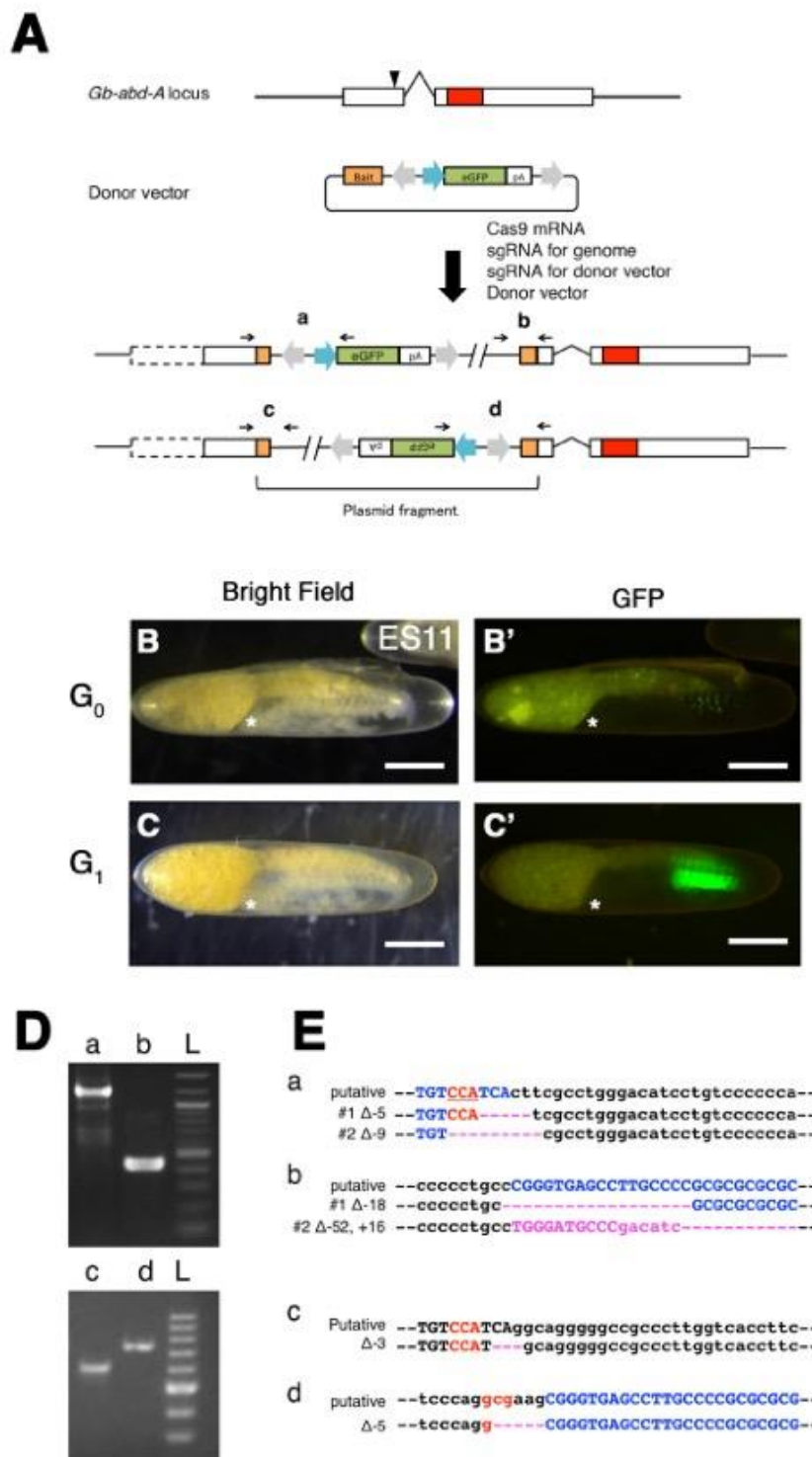
256 **Figure 3**



257

258

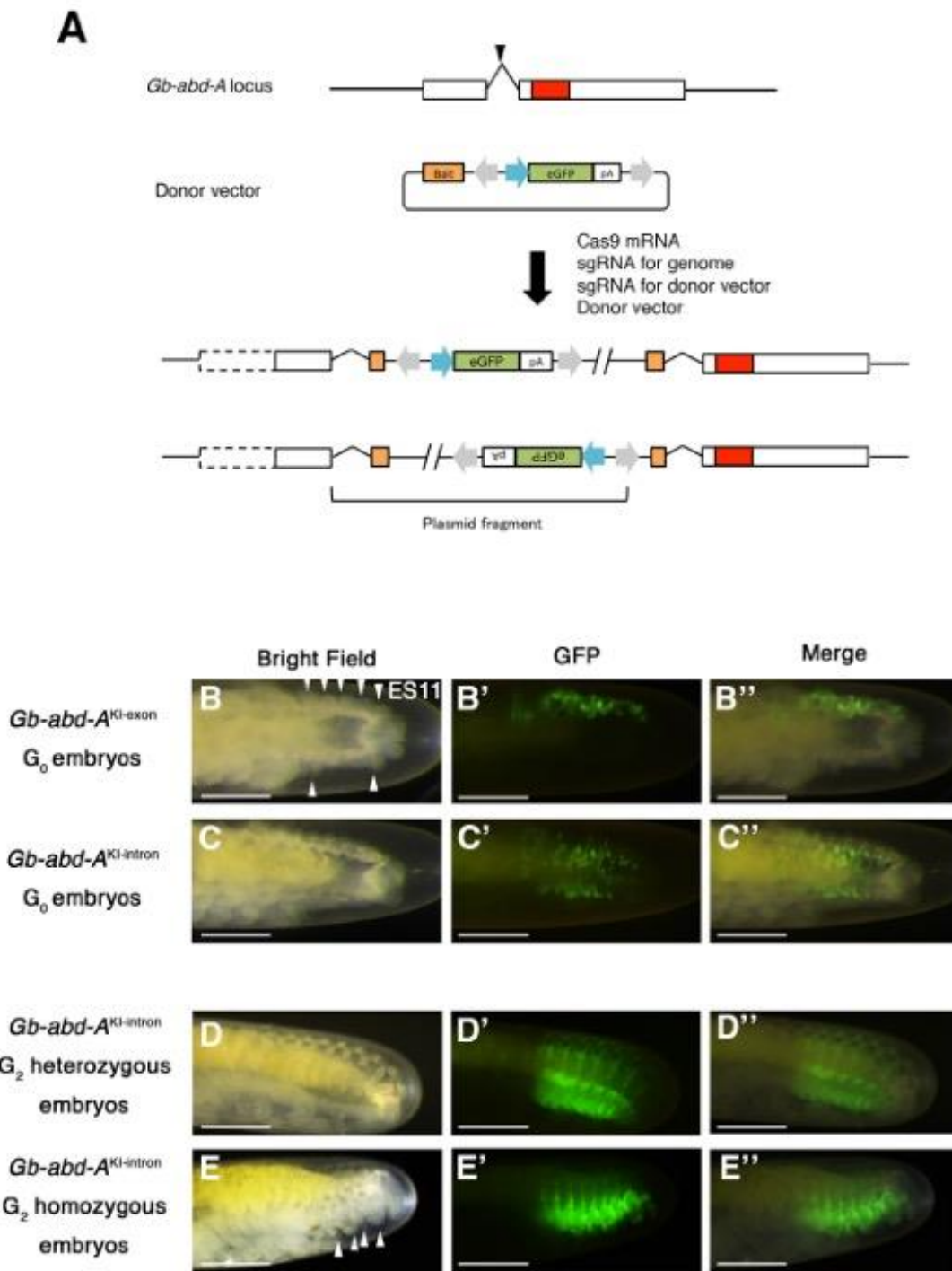
259 **Figure 4**



260

261 **Figure 5**

262



263